Summer 8-17-2018

Retreat of the Antarctic Ice Sheet in the Southern Ross Embayment from Records at Amundsen and Liv Glaciers, Southern Transantarctic Mountains

Jillian Pelto
University of Maine, jill.pelto@maine.edu

RETREAT OF THE ANTARCTIC ICE SHEET IN THE SOUTHERN ROSS EMBAYMENT FROM RECORDS AT AMUNDSEN AND LIV GLACIERS, SOUTHERN TRANSANTARCTIC MOUNTAINS

By

Jillian Nancy Pelto

B.A. Earth and Climate Sciences, University of Maine, 2015

B.A. Studio Art, University of Maine, 2015

A THESIS

Submitted in Partial Fulfillment of the

Requirements for the Degree of

Master of Science

(in Earth and Climate Sciences)

The Graduate School

The University of Maine

August 2018

Advisory Committee:

Brenda L. Hall, Professor of Earth and Climate Sciences and Quaternary and Climate Studies, Advisor

George H. Denton, Professor of Earth and Climate Sciences and Quaternary and Climate Studies

Aaron E. Putnam, Assistant Professor of Earth and Climate Sciences

Gordon R.M. Bromley, Adjunct Assistant Research Professor of Earth and Climate Sciences

RETREAT OF THE ANTARCTIC ICE SHEET IN THE SOUTHERN ROSS EMBAYMENT FROM RECORDS AT AMUNDSEN AND LIV GLACIERS, SOUTHERN TRANSANTARCTIC MOUNTAINS

By Jillian Nancy Pelto

Thesis Advisor: Dr. Brenda L. Hall

An Abstract of the Thesis Presented
in Partial Fulfillment of the Requirements for the
Degree of Master of Science
(in Earth and Climate Sciences)

August 2018

The Antarctic Ice Sheet contains ~58 m of global sea-level equivalent and thus its future behavior under global warming is of pressing concern. Examination of past ice-sheet behavior during periods of warming climate can afford insight useful for predicting future sea-level rise. This study focuses on a major unanswered question - namely, the cause of Antarctic Ice Sheet retreat following the last glaciation. Documenting the timing and nature of this deglaciation is crucial to understand the mechanisms behind ice-sheet behavior. Here, I examine how the marine portions of the ice sheet responded to the major warming that occurred at the end of the last ice age. I carried out fieldwork at Amundsen and Liv Glaciers, outlet glaciers of the East Antarctic Ice Sheet that drain through the Transantarctic Mountains to the Ross Ice Shelf. Thinning during the last deglaciation left drift on nunataks along the Ross Sea coast. My goal was to document these deposits and produce a chronology for the last stages of the most recent ice retreat. This chronology comes from radiocarbon dates of algae that lived in former ice-marginal ponds dammed by the ice sheet.

My results indicate that the Ross Sea grounding line retreated southeastward past Liv Glacier by ~4,200 yrs BP and past Amundsen Glacier by 2,900 yrs BP. Prior studies show that the deglaciation was marked by an initial period of rapid retreat, indicative of instability in this sector of the AIS. My data show that this was followed by a more gradual period of retreat in the late Holocene, with possible stabilization of the grounding line shortly after ~3000 yrs BP when it retreated to near its current position on the Siple Coast in the vicinity of Mercer Ice Stream. The timing of grounding-line retreat does not correspond closely with the largest post-LGM changes in global sea level or ocean temperature. Rather, recession was delayed significantly relative to the global deglaciation. Slowing of grounding-line retreat in the late Holocene may have been due to the effects of increased accumulation and falling local sea level, suggesting that these factors may be important in controlling the extent of the Antarctic Ice Sheet.

ACKNOWLEDGEMENTS

I first would like to extend the warmest, most heartfelt thanks to Dr. Brenda Hall for providing incredible guidance and amazing opportunities. Great appreciation also to George Denton and Aaron Putnam, my committee members, for the wonderful chance to learn and do field work in New Zealand. Thank you to Gordon Bromley for joining me in the science art exhibition “Glacially Rendered” at the Hudson Museum at the University of Maine. To all of you: your work, insight, and support have helped me immeasurably during my research.

Much appreciation to our collaborators at the University of Washington, Dr. John Stone, Joel Gombiner, Jessica Badgeley, as well as Karen Hilton, for supporting our team in the field. I’m grateful to Peter Strand for teaching me so much about geomorphology and sampling in New Zealand. Thank you to the National Science Foundation and the United States Antarctic Program for providing funding and logistical field support. Thank you to the faculty and staff of the School of Earth and Climate Sciences and the Climate Change Institute for many years of classes, field trips, adventures, and support.

I’m lucky and grateful for the friendship of my fellow graduate students, especially my office mates Courtney King, Allie Balter, and Noel Potter, for continued support. Thank you to all of my friends and family for their encouragement and assistance while I pursue this degree.

TABLE OF CONTENTS

ACKNOWLEDGEMENTS iii

LIST OF TABLES VII

LIST OF FIGURES VIII

Chapter

1. INTRODUCTION 1

    1.1 Introduction 1

    1.2 Goals and Objectives 7

    1.3 Introduction to Field Sites 8

    1.4 Methods 14

2. RESULTS 17

    2.1 Surficial Deposits at Robinson Bluff 17

        2.1.1 Robinson Bluff I Drift 17

        2.1.2 Robinson Bluff II Drift 18

        2.1.3 Robinson Bluff III Drift 19

        2.1.4 Robinson Bluff IV Drift 20

        2.1.5 Robinson Bluff V Drift 20

        2.1.6 Undifferentiated Robinson Bluff Drift 21

2.2 Surficial Deposits at Witalis Peak 23

2.2.1 Witalis Peak I Drift....................23

2.2.2 Witalis Peak II Drift 23

2.2.3 Witalis Peak III Drift....................24

2.2.4 Radiocarbon Samples 25

2.3 Surficial Deposits of Duncan Valley 28

2.3.1 Duncan Mountains Alpine Drift....................29

2.3.2 Duncan Mountains I Drift....................29

2.3.3 Duncan Mountains II Drift 31

2.3.4 Radiocarbon Samples 31

2.4 Surficial Deposits of Mt. Mason....................35

2.4.1 Mt. Mason I Drift 35

2.4.2 Mt. Mason II Drift....................36

2.4.3 Radiocarbon Samples 38

2.5 Surficial Deposits of Mt. Henson 40

2.6 Surficial Deposits of the Tusk 40

3. INTERPRETATION OF GLACIAL DEPOSITS 43

3.1 Robinson Bluff 43

3.2 Witalis Peak....................45

3.3 Duncan Mountains 46
3.4 Mount Mason 47
3.5 Mount Henson and Tusk 47
3.6 Alpine Glacier Deposits 48
3.7 Interpretation of Radiocarbon Ages 49
4. COMPARISON TO OTHER ANTARCTIC RECORDS 56
4.1 Timing of Deglaciation in the Southern TAM 56
4.2 Forcing Mechanisms 59
4.3 Implications for Behavior of the AIS 67
5. CONCLUSIONS 69
5.1 Key Findings of this Thesis 69
BIBLIOGRAPHY 71
BIOGRAPHY OF THE AUTHOR 80

LIST OF TABLES

Table 1. Dated Samples from Witalis Peak..28

Table 2. Dated Samples from Duncan Valley. 35

Table 3. Dated Samples from Mt. Mason. 40

Table 4. Forcing Mechanism Comparison. 66

LIST OF FIGURES

Figure 1. Antarctica reference map. 2

Figure 2. The Ross Embayment during the LGM. 4

Figure 3. Ross Sea region reference maps. 7

Figure 4. Field area reference maps. 9

Figure 5. Amundsen Glacier field site reference maps. 10

Figure 6. Aerial imagery of field sites. 10

Figure 7. Liv Glacier field site reference maps. 12

Figure 8. Modern algae examples. 13

Figure 9. Ancient algae examples. 13

Figure 10. Striation examples. 13

Figure 11. Ice dammed ponds. 16

Figure 12. Robinson Bluff photographs. 21

Figure 13. Robinson Bluff map. 22

Figure 14. Examples of the relatively wet and warm conditions at field sites. 22

Figure 15. Witalis Peak map. 26

Figure 16. Witalis Peak photographs. 27

Figure 17. Radiocarbon dates at Witalis Peak. 27

Figure 18. Duncan Valley map. 32

Figure 19. Duncan Valley photographs. 33

Figure 20. DMII drift. 33

Figure 21. Radiocarbon dates at Duncan Valley. 34

Figure 22. Mt. Mason photographs. 37

Figure 23. Mt. Mason map. 38

Figure 24. Radiocarbon dates at Mt. Mason..........39

Figure 25. Mt. Henson and the Tusk photographs..........41

Figure 26. Mt. Henson and the Tusk map. 42

Figure 27. Alpine glacier deposits. 49

Figure 28. Scenario 1. 51

Figure 29. Scenario 2. 51

Figure 30. Age vs. elevation graphs..........55

Figure 31. Grounding-line retreat illustration..........55

CHAPTER 1

INTRODUCTION

1.1 Introduction

The future behavior of the Antarctic Ice Sheet (AIS) under a warming climate poses one of the greatest uncertainties for global sea-level predictions. Because the ice sheet contains a volume equivalent to ~58 m of global sea level, the amount and pacing of its contribution to sea-level rise is of major societal concern (Fretwell et al., 2013). Currently, the AIS consists of the marine-based West Antarctic Ice Sheet (WAIS; ~3.3-4.3 m global sea-level equivalent) and the primarily terrestrial-based East Antarctic Ice Sheet (EAIS; ~53.3 m global sea-level equivalent; Figure 1)(Bamber et al., 2009; Fretwell et al., 2013) Most concern focuses on the WAIS, which is thought to be potentially unstable given that much of the ice sheet is grounded below sea level and its bed becomes deeper inland (Hughes, 1973; Mercer, 1978; Weertman, 1974, 1976). Rapid grounding-line retreat and possibly even incipient ice-sheet collapse may already be underway at Thwaites and Pine Island Glaciers in the Amundsen Sea sector of West Antarctica (Joughin et al., 2014a; Rignot et al., 2014) as a result of warm Circum-Polar Deep Water circulating to the grounding lines. More widespread warming of the Southern Ocean in the future could cause collapse to spread to other sectors of the WAIS. In addition, there is considerable worry about the health of ice shelves that buttress and protect the WAIS. Mercer (1978) predicted that warming climate would lead to loss of ice shelves from north to south. culminating in the breakup of the Ross Ice Shelf (RIS) and ultimately the demise of the WAIS. Collapse of numerous Antarctic Peninsula ice shelves over the past few decades may represent the first stages of this scenario (Cook & Vaughan, 2010; De Angelis & Skvarca, 2003; Scambos et al., 2004; Skvarca et al., 2004).

In contrast, the terrestrial EAIS is generally thought to be stable (Denton et al., 1993). However, some suggest that under intervals of warmth, such as the Pliocene, this ice sheet also may have undergone collapse (Cook et al., 2013; Pollard et al., 2015; Scherer et al., 2016), leading to higher global sea levels (Miller et al., 2012). In addition, an important question is whether ice from West Antarctica buttresses a significant amount of ice flow from East Antarctica through a region called the Bottleneck. If it does, a collapse of the WAIS could drastically affect the drainage of the EAIS and cause interior draw down of ice (Hughes, 2009). Alternatively, others suggest that during past intervals of warmth, the EAIS remained stable and was even more extensive than at present (Denton et al., 1993; Winnick & Caves, 2015).

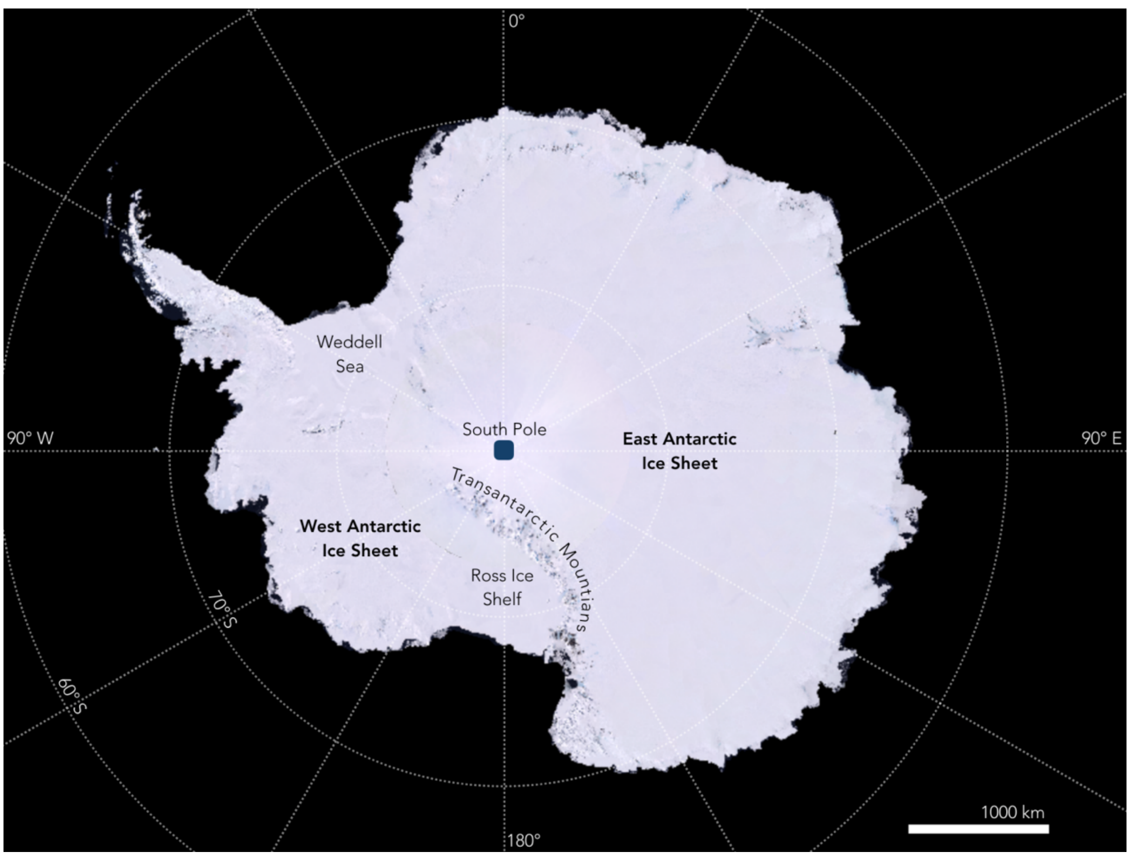

Figure 1. Antarctica reference map. Base image from the Polar Geospatial Center Antarctic Imagery Viewer.

The behavior of the AIS during the global last glacial maximum (LGM; ~26,500-18,000 yrs BP) and deglaciation affords clues as to the mechanisms that control ice-sheet extent. Reconstructions of the AIS during the global LGM show limited inland ice thickening and a large expansion of ice onto the continental shelves (Figure 2; Denton & Hughes, 2000). In the Ross Embayment, the lower reaches of outlet glaciers from the EAIS and the ice streams from the WAIS coalesced to create an expanded ice sheet grounded close to the north edge of the Ross Sea (Anderson et al., 2014; Denton & Hughes, 2000, 2002; Hall & Denton, 2000). Evidence of former ice-sheet extent comes from terrestrial deposits, such as drifts and glacial erratics in the Transantarctic Mountains (TAM), and from landforms on the sea floor (Anderson et al., 2014; Denton & Hughes, 2002; Hall & Denton, 2000). Deposits at the coast of the southernmost TAM suggest ice-sheet surface elevations of ~1100 m at both Reedy and Scott Glaciers (Bromley et al., 2010, 2012). Farther north, ice surface elevations were similar, ~1000 m at the mouth of Beardmore Glacier and 900 m at Hatherton Glacier (Anderson et al., 2004; Bockheim et al., 1989; King, 2017; Spector et al., 2017). Longitudinal ice-surface profiles of TAM outlet glaciers show that most ice thickening occurred near the coast, with less change at the inland heads of the glaciers. The greater thickening at the mouths was due largely to the buttressing effect of grounded ice in the Ross Sea. During deglaciation, the reduction in backstress due to down draw and grounding-line retreat in the Ross Sea caused thinning to occur sooner at the mouths of outlet glaciers than at upstream locations (Jones et al., 2015). This behavior resulted in a time-transgressive maximum, with local LGM positions attained sooner towards the coast than inland. This effect was compounded by an increase in accumulation during the ice-age termination and the Holocene (Cuffey et al., 2016), which further delayed the local glacial maxima and recessions at inland locations (Hall et al., 2015). For example, the maximum ice elevation at

Reedy Glacier occurred between 14,000-17,000 yrs BP in the Quartz Hills near the junction with Mercer Ice Stream but at ~7,000 yrs BP near the EAIS plateau (Bromley et al., 2010; Todd et al., 2010). Thus, outlet glacier behavior is governed by multiple factors, with local accumulation and marine down draw playing important roles.

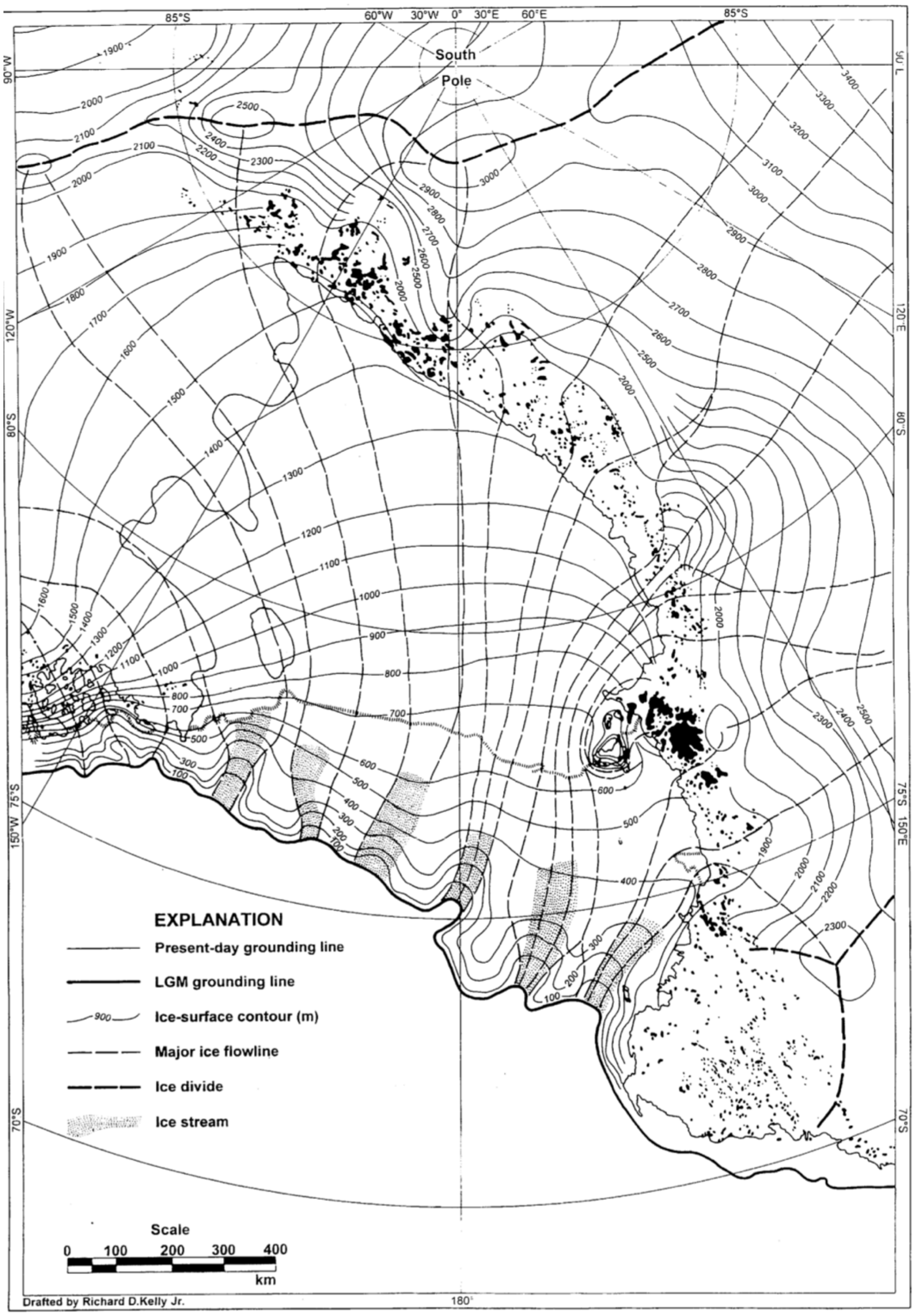

Figure 2. The Ross Embayment during the LGM. This is a reconstruction from Denton and Hughes (2000) of the extent and elevation of the ice sheet during the LGM, based largely on glacial geologic evidence.

There is disagreement about the behavior of the AIS during the last deglaciation. Based on an interpretation of ice-rafted debris in the Scotia Sea, Weber et al. (2014) suggested that the ice sheet underwent periodic unstable behavior during the LGM and deglaciation, including a collapse of one or more sectors. One of these postulated collapses is thought to have contributed as much as 18 meters of global sea level during meltwater pulse 1a (MWP1a) at ~14,650 - 14,310 yrs BP (Deschamps et al., 2012). Bassett et al. (2007) used sea-level change predictions from the Antarctic coast and deglacial records with a spherically symmetric earth viscosity model to show that MWP1a could have been sourced from ice in the Weddell and Ross Seas, as well as from the Antarctic Peninsula. However, neither the timing of MWP1a nor the volume of sea-level change required matches the deglacial reconstructions of the AIS discussed below (Ackert et al., 1999; Hall et al., 2013; Licht, 2004).

An alternate view is that Ross Sea deglaciation occurred almost entirely during the Holocene, much later than Pleistocene deglaciation of the southern mid-latitudes which occurred at ~17,500 yrs BP (Denton et al., 2010) and after the MWP1a signal (Conway et al., 1999; Hall et al., 2013; Jones et al., 2015; Spector et al., 2017). EAIS outlet glaciers in the Transantarctic Mountains lack evidence for significant thinning until after ~13,000 yrs BP, and rapid thinning was not underway until ~9,000 yrs BP (Hall et al., 2013; Spector et al., 2017; Todd et al., 2010). Grounding-line retreat is thought to have occurred primarily in the early Holocene in the northern Ross Sea, with deglaciation to Beardmore Glacier by at least 7,000 yrs BP (Baroni & Hall, 2004; Hall et al., 2004; Mckay et al., 2008; Spector et al., 2017). However, despite prior work, the timing and nature of grounding-line retreat from its maximum position on the continental shelf to its current location on the Siple Coast remain unclear and are a subject of this present study. At present, there is very little chronologic control on the history of ice retreat south of Beardmore Glacier (Conway et al., 1999; Hall et al., 2013; Spector et al., 2017). Yet, the last few thousand years of ice recession afford important context for present and future ice-sheet behavior. Specific questions addressed by my work include: When did deglaciation occur in the southern Ross Embayment? Was deglaciation of the Ross Sea Embayment a single rapid event that took place between about 7,000-9,000 yrs BP, perhaps as a result of unstable ice-sheet behavior? Or did deglaciation slow and become more gradual in the late Holocene? When did the WAIS grounding line retreat south to its current location on the Siple Coast? Is there any evidence of late Holocene readvance? What caused the grounding-line changes? Does the timing of grounding-line retreat correspond to changes in sea level, ocean temperature, and/or accumulation?

The field sites in this present study lie between Beardmore and Scott Glaciers, in a 400 km coastal stretch of the TAM, where there currently is a lack of data bearing on the timing of grounding-line recession (Figure 3). Thus, my work will be able to address some of these questions about the nature of Holocene retreat in the southern Ross Embayment and allow me to begin to constrain the mechanisms behind ice-sheet thinning and eventual grounding-line retreat. Further, addressing these questions will help us to understand the recession history, and thus potentially the stability, of the WAIS and may provide context for future predictions.

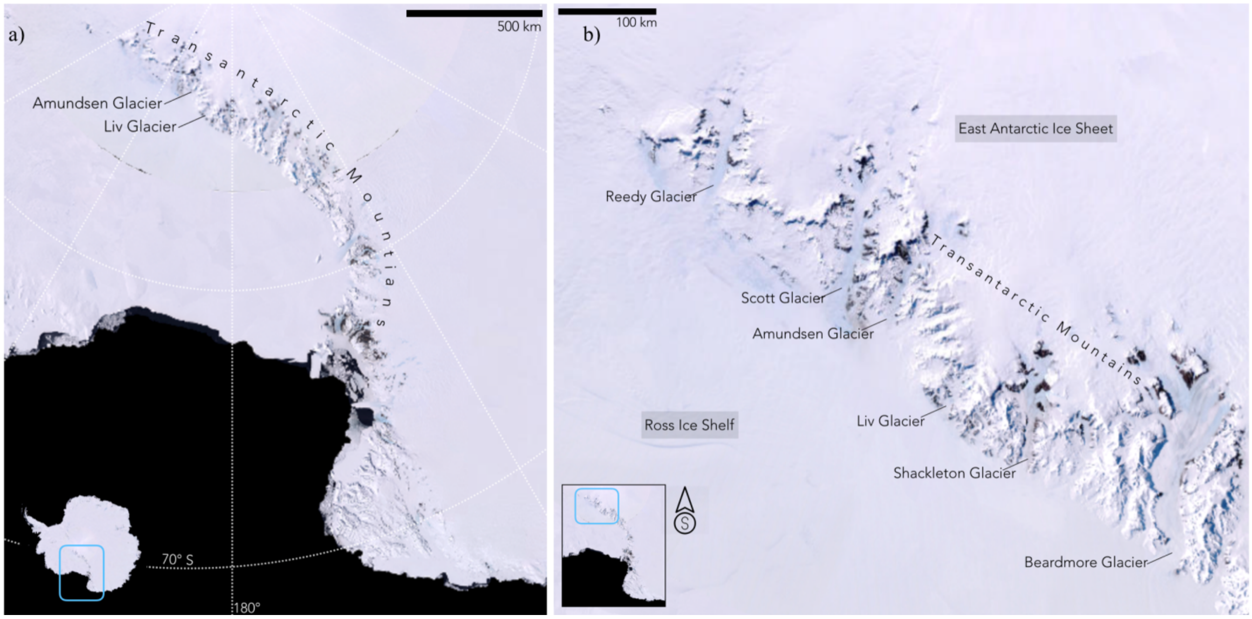

Figure 3. Ross Sea region reference maps. a) The Ross Embayment with Amundsen and Liv Glaciers labeled. b) The southern Transantarctic Mountains, with key outlet glaciers labeled. Base image from the Polar Geospatial Center Antarctic Imagery Viewer.

1.2 Goals and Objectives

The overall goal of this research is to understand better the recent history of the AIS as a means of assessing not only the mechanisms controlling ice-sheet extent, but also its likely future. The particular goal of this study is to document the history of ice recession in the southern Ross Sea Embayment, particularly late Holocene thinning and grounding-line retreat. I address these goals using the following objectives:

1. Determine former ice extent, elevation, and flow direction during the LGM and deglaciation in the southern Ross Sea Embayment, specifically near the termini of Amundsen and Liv Glaciers.

2. Develop a chronology that addresses the timing and nature of late Holocene recession near Amundsen and Liv Glaciers, including final ice thinning and southward grounding-line retreat in the Ross Embayment.

3. Provide insight into the causes of deglaciation in the Ross Sea Embayment and the ways in which these mechanisms may affect the WAIS under future global warming.

1.3 Introduction to Field Sites

I focused on the southwestern Ross Sea Embayment near the termini of Liv and Amundsen Glaciers. The chosen study sites at nunataks in the TAM preserve a record of the final thinning of the glaciers, which took place when their termini reached the point of flotation. This flotation occurred as the Ross Sea grounding line migrated southward past the glacier mouths and grounded ice was replaced by the floating ice shelf.

The field seasons for this project took place at Amundsen Glacier in December and January of 2016-17 and at Liv Glacier in December and January of 2017-18. Specific nunataks were chosen based on their positions close to the termini of major outlet glaciers, their accessibility, the presence of ice dammed-ponds, and the potential for glacial deposits that mark the thinning of the ice to its present position.

We visited two nunataks at Amundsen Glacier (Figures 4-6), which drains the EAIS through the TAM to the RIS. Robinson Bluff (~85.59°S, ~159.91°W; 3.2 x 2.4 km; Figure 5a) is located about 24 km up-glacier from the RIS. It consists of a high bedrock ridgeline with ~500 m of relief partially encircling a central valley, which trends north to south. The nunatak is bordered upstream by the confluence of Amundsen Glacier and the small tributary, Whitney

Glacier. A small unnamed tributary glacier — hereafter termed Robinson Glacier — flows on the northern side of the nunatak (Figure 5a). Several small ponds are dammed against the east and north facing edges of Robinson Bluff. Bedrock is primarily granite/granite gneiss, with some regions of hornblende gabbro on the eastern ridge (Burgener, 1975).

The second site, Witalis Peak (~85.53°S, ~160.24°W; 4.5 x 2.7 km; Figure 5b), is located about 16 km up glacier from the RIS, adjacent to the grounding line of Amundsen Glacier. The peak forms part of a ridgeline that curves around an east-west trending valley. The confluence of Amundsen and Robinson Glacier occurs on the southeast side of the nunatak; the combined Steagall and Bowman Glaciers flow along its northern side (Figure 5b). Several ponds are dammed against the northeastern facing slopes of Witalis Peak. Bedrock is a banded gneiss, with biotite-rich and quartz- and feldspar-rich components(Burgener, 1975).

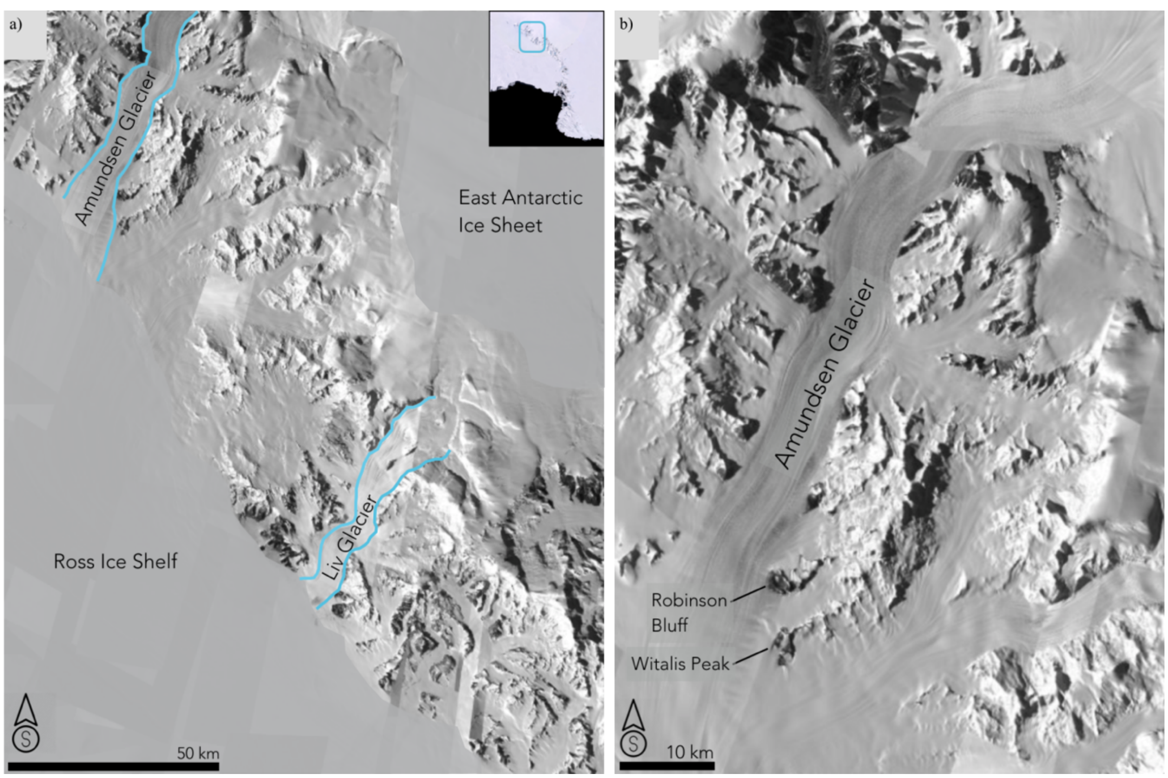

Figure 4. Field area reference maps. a) Amundsen and Liv Glaciers, outlet glaciers of the EAIS flowing through the TAM to the RIS. b) Amundsen Glacier and our two field sites, Robinson Bluff and Witalis Peak. Base image from the Polar Geospatial Center Antarctic Imagery Viewer.

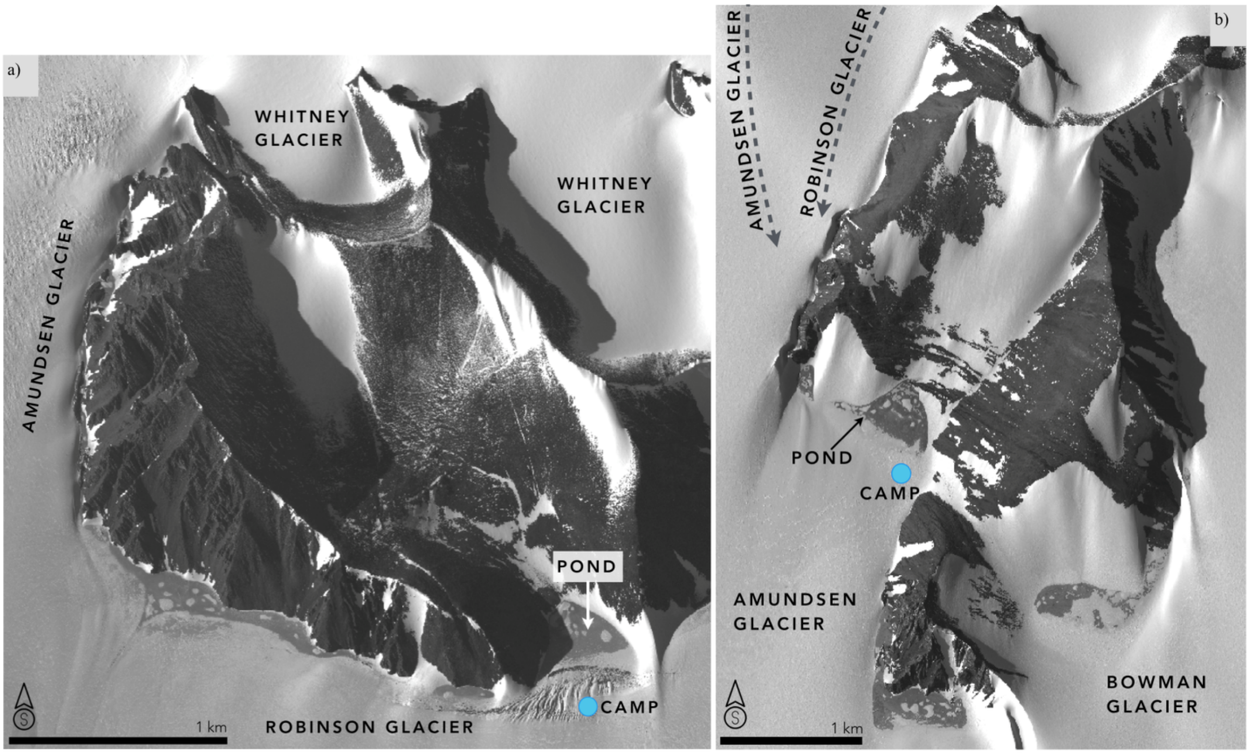

Figure 5. Amundsen Glacier field site reference maps. a) Robinson Bluff. b) Witalis Peak. Satellite imagery from the Polar Geospatial Center.

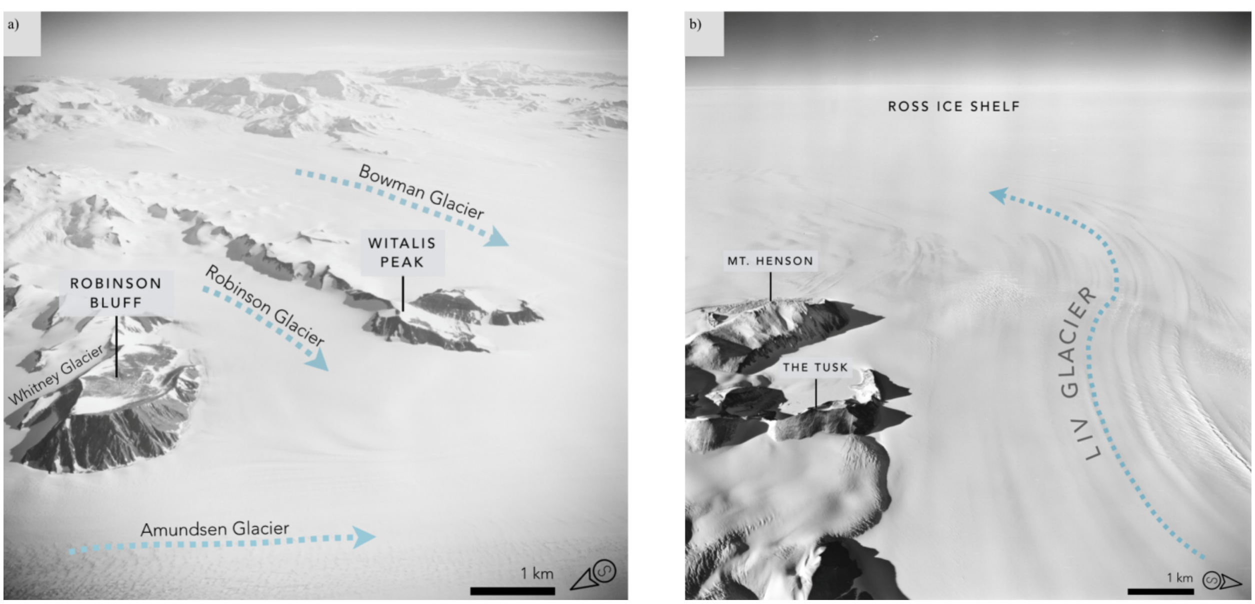

Figure 6. Aerial imagery of field sites. a) Robinson Bluff and Witalis Peak. b) Mt. Henson and the Tusk.

We also carried out work at and near Liv Glacier (Figures 6b, 7), an outlet glacier of the EAIS, approximately 80 km north along the TAM from Amundsen Glacier. We worked at nunataks adjacent to either side of the glacier mouth, as well as along the coast to the north of Liv Glacier.

The Duncan Mountains (~84.96°S, ~166.54°W; 26 x 10 km; Figures 7b) are adjacent to the RIS to the south of Liv Glacier. Our field site consists of a high bedrock ridgeline (~1000 m of relief) around a central valley (hereafter termed Duncan Valley - 4 km long x 1 km wide) that trends northeast to southwest. The nunatak is bordered by Somero Glacier, a tributary to Liv Glacier, along its inland side (Figure 6b). Several large ponds are dammed against the north-facing slopes of the Duncan Mountains. Bedrock is primarily schist, but there may also be regions of gneiss and granite (McGregor, 1965).

Mt. Mason (~84.70°S, ~170.08°W; 5 x 3.5 km; Figure 7c) is located ~ 2 km inland of the RIS, ~20 km northwest of Liv Glacier. The peak (~816 m elevation) forms part of a ridgeline with two arms extending on either side of a northwest-to southeast-trending valley. The nunatak is bordered to the north by Le Couteur Glacier and to the south by Morris Glacier (Figure 6c). Two large ponds, separated by a bedrock ridge, are dammed against the nunatak. Bedrock is primarily granite and granodiorite (McGregor, 1965).

Mt. Henson (~84.84°S, ~168.39°W; 4.5 x 2.5 km; ~900 m elevation; Figure 7d) is located at the edge of the RIS, adjacent to the northern side of Liv Glacier. A small pond is dammed against the northern side of the mountain. Granodiorite and marble make up the local bedrock (McGregor, 1965). About 1.6 km to the south, another field site, The Tusk (84.87°S, ~168.26°W; 2.5 x 1.8 km; Figure 6d), is located adjacent to the left-lateral margin of Liv Glacier

~7.5 km from the glacier terminus. A large pond also is dammed against the northern side of The Tusk, which is primarily marble, with some regions of granodiorite (McGregor, 1965).

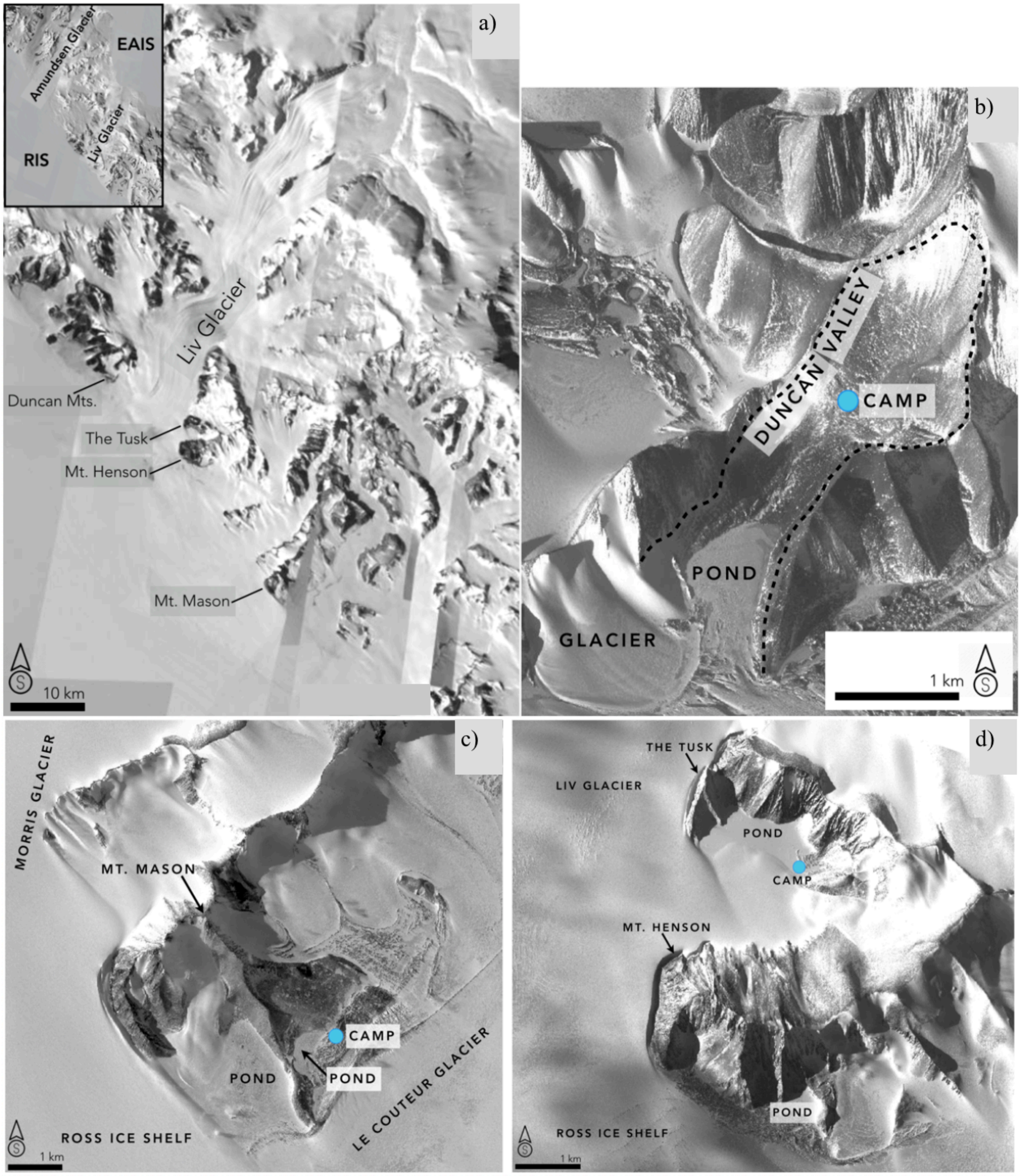

Figure 7. Liv Glacier field site reference maps. a) Liv Glacier and adjacent field sites labeled. b) Duncan Valley. c) Mt. Mason. d) Mt. Henson and the Tusk. Satellite imagery from the Polar Geospatial Center.

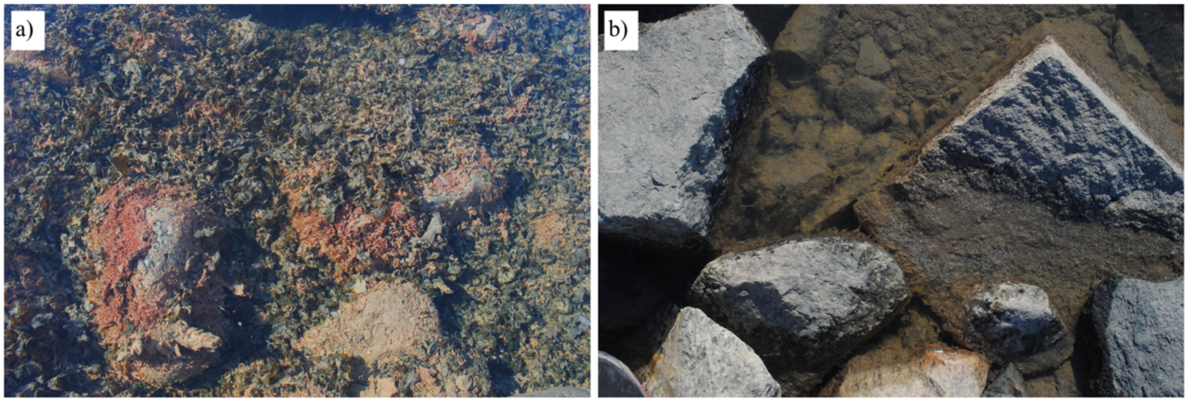

Figure 8. Modern algae examples. Photographs at Mt. Mason of three different types of modern algae. a) Two different types of algae covering the bottom of a small pool in the valley. b) One type of algae found in the large pond.

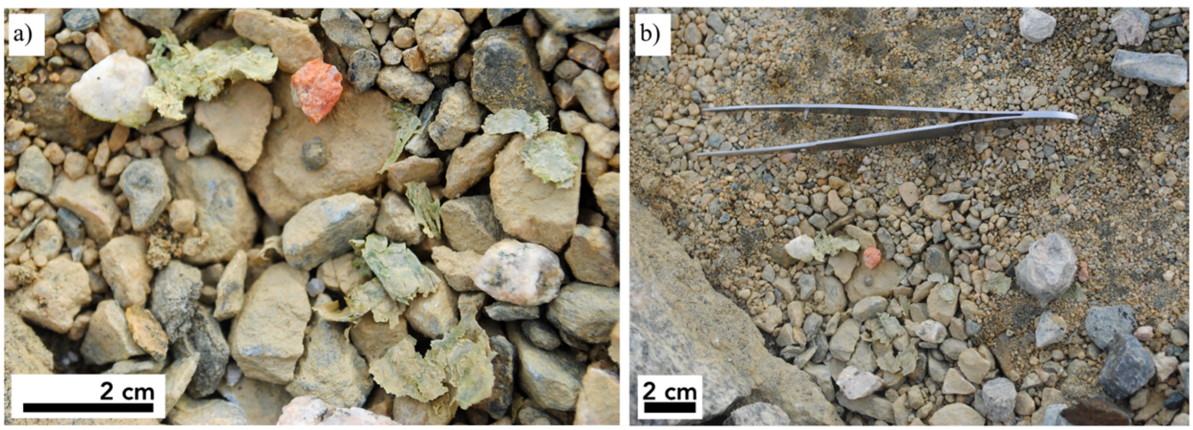

Figure 9. Ancient algae examples. Photographs at Witalis Peak of algae we sampled. a) This sample was found within this sand and gravel, underneath a small cobble. b) the same sample in (a) showing the surface underneath the cobble where the algae was found, with our sampling tweezers for scale.

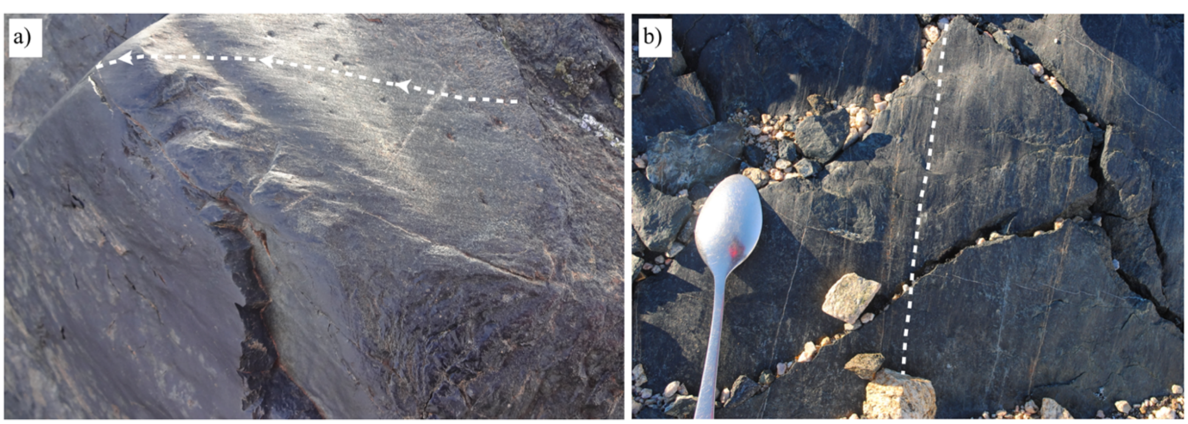

Figure 10. Striation examples. a) Stoss and lee forms on striated bedrock at Witalis Peak. b) striations on bedrock at Witalis Peak.

1.4 Methods

Fieldwork consisted of mapping glacial deposits to delineate past ice margins, measuring striations to reconstruct former ice flow, collecting ancient algae samples from glaciolacustrine deposits for ^{14}C dating, and sampling erratics from ridgelines for ^{10}Be exposure-age dating. My focus is on geomorphic mapping, flow reconstructions, and radiocarbon dating; our collaborators at the University of Washington will conduct ^{10}Be dating.

For each field location, I used ArcMap to document the surficial geology on satellite imagery with 0.5 m resolution from the Polar Geospatial Center and improved the mapping by an extensive field survey. The field mapping included noting the extent, elevation, composition, and morphology of drifts, as well as the location of former ice-marginal pond basins. We also examined drift grain size and lithology, as well as relative weathering differences, including the degree of staining, pitting, and exfoliation of rock surfaces. We also the measured striation orientations on bedrock; direction of flow was determined in several locations by examining molded stoss and lee forms (Figure 10).

To develop a chronology for deglaciation, I collected ancient algae from former ice-marginal pond basins and/or shorelines. Today the glaciers dam ponds at the ice-rock edge, particularly where lateral distributary lobes enter ice-free valleys. These ponds often contain seasonally open areas of water (moats) where algae can live (Figures 8, 11). Pond formation is dependent on melting in radiation traps adjacent to the glacier margin, as well as on wind scouring and temperature enhancements from descending katabatic winds (Parish & Bromwich, 1998; Vihma et al., 2011; Zwinger et al., 2015). When Amundsen and Liv Glaciers were thicker than they are at present, they also dammed ice-marginal ponds. As the ice thinned to its present location, ponds followed the ice margin and moved downslope. Algae from these ponds remain stranded on the hillsides, recording not only the position of former ponds, but also information about the former ice margins (Figures 9, 11). The elevation of an algae sample represents the minimum elevation of the pond, as well as the minimum elevation of the ice necessary to dam the pond. Thus, radiocarbon ages of the algae afford a chronology for former ice positions (Hall et al., 2016; King, 2017). Moreover, the presence of algae indicates that the sites where they grew were free of glacier ice at that time. Evidence of ponds on hillsides well above the modern water bodies is an immediate indicator of more extensive and/or thicker ice, since a pond could not have existed on a slope without an ice dam.

Fifty-nine algae samples, 17 from sites at Amundsen Glacier and 42 from sites near Liv Glacier, were sent for radiocarbon dating. For each sample I submitted ~20 mg of algae to the National Ocean Sciences Accelerator Mass Spectrometry (NOSAMS) Laboratory at Woods Hole Oceanographic Institute. Samples were subjected to standard acid-base-acid pretreatment before being converted to graphite and pressed into a target for the accelerator. Stable ^{13}C was measured for each sample. The ^{14}C dates were converted to calendar years with a 1-sigma error in CALIB 7.10 using the INTCAL13 calibration curve (Reimer et al., 2013). All dates presented here are in calendar ages. To assess a possible reservoir effect, I collected water from the open moats and in the field added barium hydroxide octahydrate, which dissociates and binds rapidly with the CO_2 in the water, causing barium carbonate to precipitate (Hendy & Hall, 2006). We then dated the carbonate, which tells us whether CO_2 in the water has equilibrated with the atmosphere or if there is a lake reservoir effect. A lake reservoir effect could come about from carbonate minerals or from CO_2 from ancient air bubbles in the melting glacier ice adjacent to the lake.

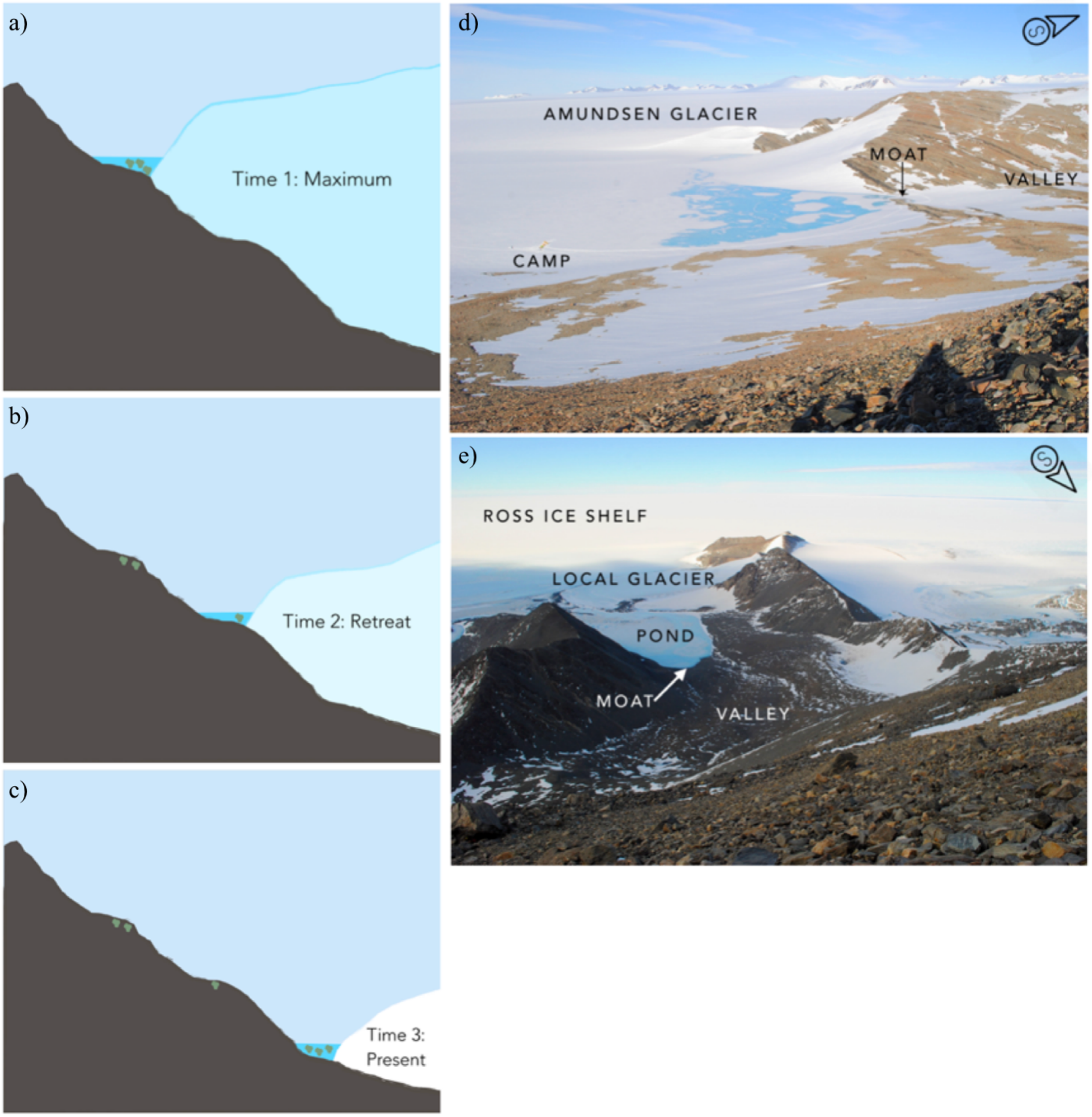

Figure 11. Ice dammed ponds. a) Time 1: Ice at its maximum extent dams a pond high on the hillside. Algae lives in this pond. b) Time 2: Ice has retreated down the slope from its maximum extent, and a new pond is dammed at this position. Algae that lived in the pond in Time 1 are now preserved on the slope. c) Time 3: Ice in its present position, damming the modern pond in which algae live. d) An ice-dammed pond at Witalis Peak. e) An ice-dammed pond at Duncan Valley.

CHAPTER 2

RESULTS

2.1 Surficial Deposits at Robinson Bluff

I identified six distinct drifts at Robinson Bluff. Four of these extend in lobes that trend southward through the central valley from Robinson Glacier, as well as westward onto the nunatak from Amundsen Glacier. All of these deposits overlie an undifferentiated drift whose source is uncertain. Finally, there is also a modern drift on and immediately adjacent to Robinson Glacier, as well as adjacent to a local alpine glacier. Throughout the valley, all of the drifts show evidence of re-working from periglacial activity, including solifluction lobes, stone sorting, and clasts reoriented by creep (Figure 13).

2.1.1 Robinson Bluff I Drift

Robinson Bluff I (RBI) drift is composed of recent and currently active deposits. Notable among these is a moraine forming today at the right-lateral edge of Robinson Glacier, adjacent to the ice-dammed pond at 405 m elevation. This moraine has a steep ice-contact slope (3-5 meters high) and a gentle ice distal side (0.5-2 meters high). A sheet of scattered erratics occurs as much as 190 m distal to this moraine. Both deposits are composed of ~95-99% granite and ~1-5% fine-grained mafic dike rock. Most of the deposit is lightly weathered, although some rocks have moderate staining. Most boulders that appear very fresh have evidence of exfoliation. The grain size varies from small cobbles to medium-sized boulders, and the rocks are angular to sub-angular.

RBI drift also forms three small left-lateral moraines adjacent to an alpine glacier that descends from the southwestern ridgeline. The site was not examined in detail, but the rocks appear to be primarily granitic, angular, and with little to no staining.

2.1.2 Robinson Bluff II Drift

Robinson Bluff II (RBII) drift occurs in three separate regions of the nunatak. I correlate deposits among these sites based on their extent, elevation, weathering characteristics, and position relative to the other drifts.

The most expansive portion of this drift sheet extends from the modern ice-dammed pond at Robinson Glacier southward through the central valley to a clear limit at ~590 m elevation on the northeastern ridge. This limit is marked by a distinct change in weathering and, in places, by an elongated snow patch following an ice-marginal terrace. The drift edge descends in elevation up valley and is well-delineated by a large bouldery moraine (4-8 m relief) at ~585 m elevation where it crosses the valley floor (Figure 12c). Proximal to this moraine, there are ~28 terrace scarps, most of which cross the valley. They have ~1 to 3 m of relief. RBII drift in the valley is thick, with abundant evidence of periglacial activity, including solifluction lobes, nivation hollows, and stone sorting. The drift is grey in color and is a diamicton with a grain size ranging from sand to large boulders. About 98% of the rocks are granitic; the remaining clasts include granodiorite, rock from local mafic dikes, and foliated granite-gneiss. Overall, the deposit is lightly weathered and is less consolidated than deposits just upslope.

A second deposit of RBII drift extends northward across the eastern ridgeline of the nunatak at ~599 m elevation and descends into the central valley as a lobe of drift. This lobe commonly is draped over the more stained RBIII drift and is marked by a steep, narrow, black moraine (1-2 m relief) whose toe is at ~568 m elevation (Figure 12c). Aside from the demarcation by the black moraine at the toe of the drift lobe, the limits of this deposit are approximate and marked only by the change in density of black mafic rock to the outboard granitic rocks. Inboard of the drift limit, a series of small arcuate moraines descends through cols toward the central valley. This deposit of RBII drift is composed of cobbles to very large boulders, with rock types of approximately equal parts of gabbro and granite/granite gneiss. Most clasts appear lightly weathered.

The third deposit of RBII drift extends from Whitney Glacier to just below the southern ridgeline of Robinson Bluff at 849 m elevation. Twenty or more small ice-marginal terraces with about one-half to one meter of relief and a steep ice-contact slope facing Whitney Glacier, extend across the slope.

2.1.3 Robinson Bluff III Drift

Robinson Bluff III (RBIII) drift extends up valley from the RBII drift edge and can be traced onto the eastern ridgeline to ~620 m elevation, where it is differentiated from older drifts upslope by changes in weathering and grain size. In the valley, the drift terminates at a sequence of closely spaced moraines at ~600 m elevation. These moraines differ from the younger RBII deposits located just downslope in that they have a smaller grain size (although there are some large boulders) and rocks that are more stained and weathered. The moraine is stable with few void spaces, although there are some perched boulders. About 75% of the clasts are granite/granite gneiss and 25% are mafic rocks (gabbro, diorite, dark grey gneiss). RBIII drift is stained orange and many rocks show exfoliation. This deposit has been modified by periglacial activity.

2.1.4 Robinson Bluff IV Drift

Robinson Bluff IV (RBIV) drift extends from the upslope limit of RBIII drift to the eastern ridge line, where the limit is marked by a visible weathering change. Overall, this deposit looks older than RBIII drift, with increased weathering, staining, and exfoliation. There are few boulders, and the deposit surface appears hummocky. Rocks are primarily granite to granitic gneiss, with a shift to more gneiss upslope. Most landforms appear to be due to solifluction rather than to glacial deposition.

2.1.5 Robinson Bluff V Drift

Robinson Bluff V (RBV) drift extends across the central valley from the limit of RBIV drift upward to the modern valley glacier, and on part of the eastern valley wall, terminating close to the ridgeline. The contact between RBV drift and the undifferentiated drift upslope is defined only by a transition to an older-looking surface which has no associated landforms or evidence of ice-flow direction. Periglacial activity is evident across this drift.

RBV drift has only one distinct moraine, located just upslope of the RBIV drift limit on the western side of the valley, at ~637 m elevation. The moraine is about one meter in height and extends laterally 500 m. In addition, a series of poorly preserved scarps, either moraines or ice-contact terraces, occur on the western valley wall.

RBV drift is composed of granite and granite-gneiss clasts, primarily of cobble size. Rocks are sub-angular, with more rounding than those located just downslope. The degree of weathering is very high, with heavy staining and exfoliation.

2.1.6 Undifferentiated Robinson Bluff Drift

Drift deposits on Robinson Bluff distal to RBV drift are undifferentiated due to a lack of landforms or other signifying characteristics. The drift appears to underlie the other valley deposits.

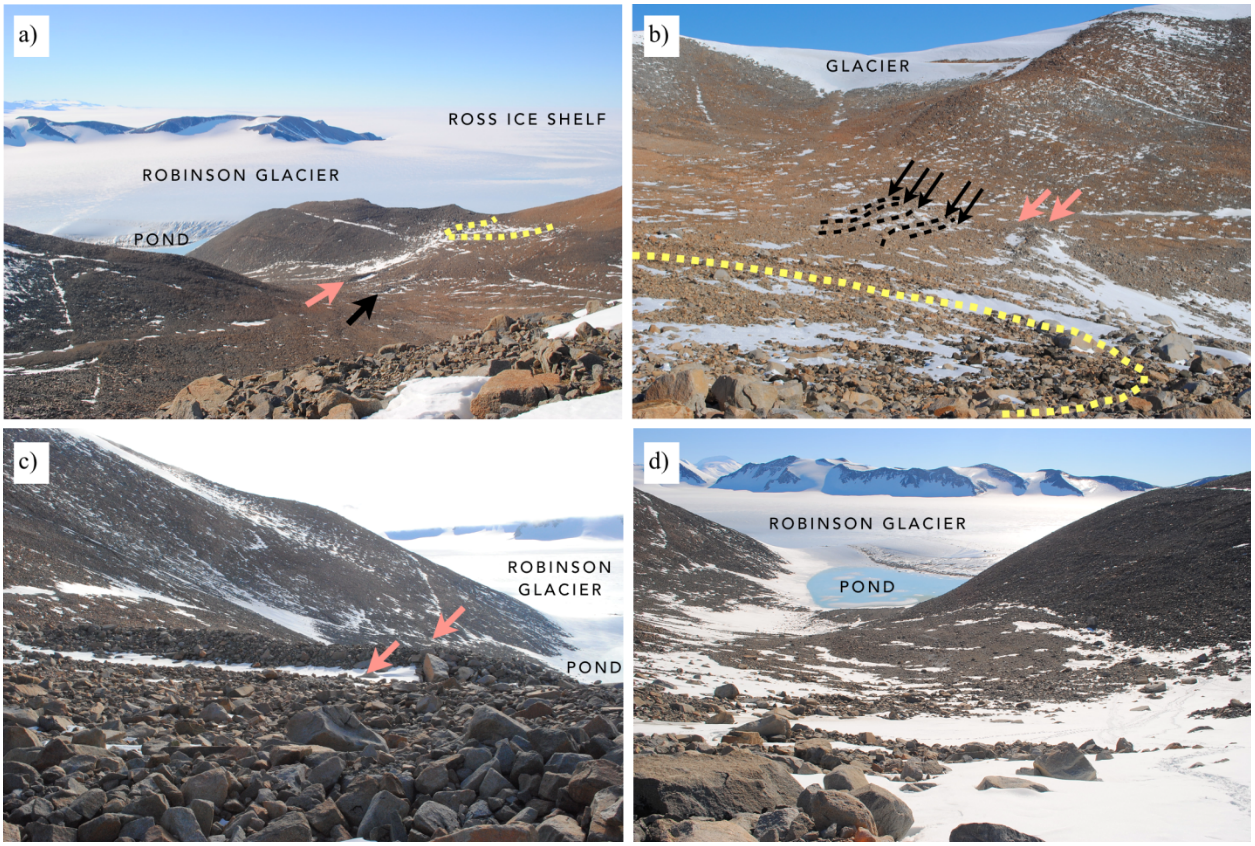

Figure 12. Robinson Bluff photographs. Orange arrows mark the bouldery moraine at the transition from RBII to RBIII drifts. Yellow dashed line marks the RBII moraine that extends from the east ridge. Black arrow and dashed lines represent a series of moraines in RBIII drift. a) View from the west ridge of the valley. b) View from the east ridge towards the west ridge; modern glacier labeled. c) The bouldery moraine with the more prominent crest and the outboard smaller crest noted by the arrows. d) View of RBII ice-marginal terraces on the slope leading up to the moraine in (c).

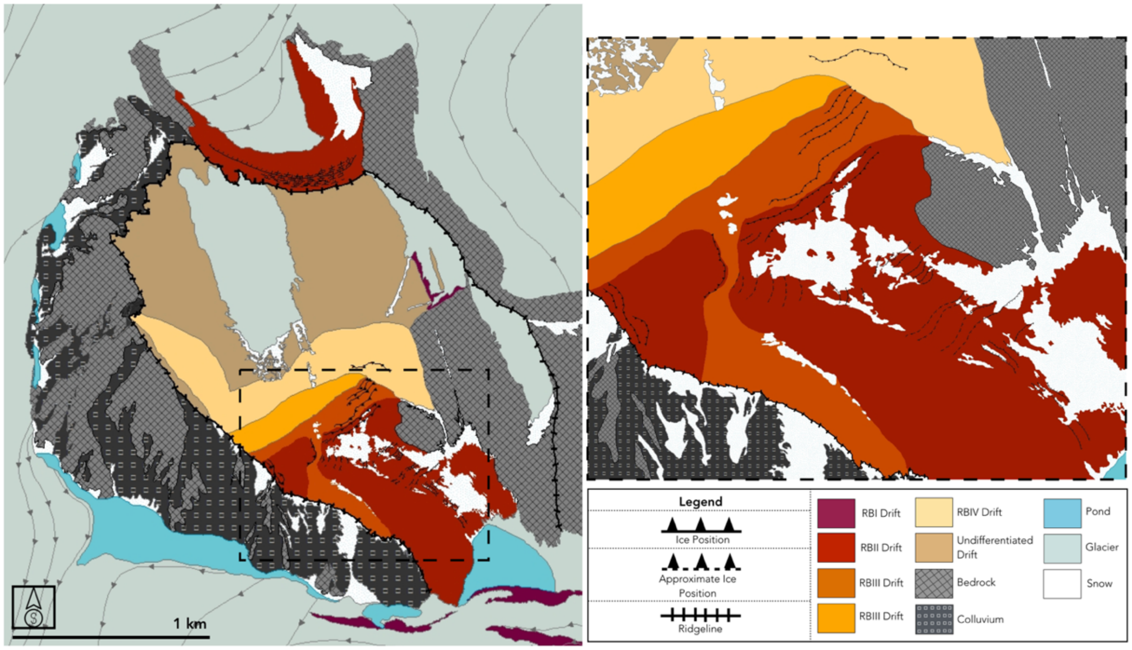

Figure 13. Robinson Bluff map. Surficial geologic map based on field observations, using satellite imagery from the Polar Geospatial Center. Inset image shows moraines and terraces in RBII-V drifts.

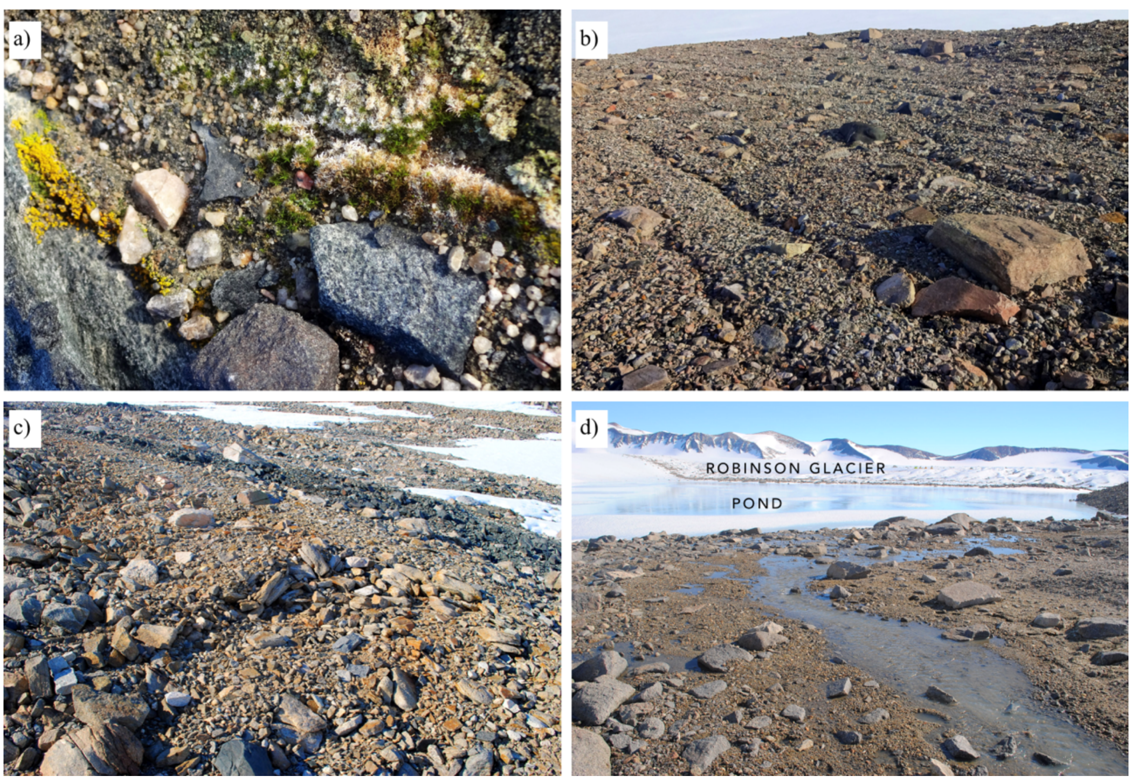

Figure 14. Examples of the relatively wet and warm conditions at field sites. a) Moss and lichen at Witalis Peak. b) Periglacial features, potentially the beginning of stone stripes, at Witalis Peak. c) Sorted polygons at Witalis Peak. d) Meltwater channels at Robinson Bluff.

2.2 Surficial Deposits at Witalis Peak

I identified two distinct drifts at Witalis Peak, as well as modern deposits on Bowman Glacier. In general, drift cover is thin on the nunatak, and exposed, frost-shattered bedrock is common. Throughout most of the valley, there is evidence, such as solifluction lobes and sorted polygons, of re-working of deposits from periglacial activity (Figure 13).

2.2.1 Witalis Peak I Drift

Witalis Peak I (WPI) drift consists of deposits forming on Bowman Glacier below the northern ridgeline of the nunatak. The drift extends as much as 500 m inboard from the glacier margin and consists largely of rockfall from the cliff, which is forming an ice-cored moraine. We did not descend this ridge as it is steep and eroding, so the composition and characteristics of this feature are uncertain.

2.2.2 Witalis Peak II Drift

Witalis Peak II (WPII) drift extends from the modern ice-dammed pond at the bottom of the valley (~272 m elevation) to ~330 m elevation in the central valley and to ~440 m elevation on the eastern ridge (Figure 14). I define the map unit as the extent of lightly to moderately weathered erratics. There are no clear drift limits nor landforms; however, glacial polish and striations are common (Figure 10). Striations on bedrock range primarily from ~45º-60º (where 0º is set as north), measured at more than 20 sites. The bedrock also displays polish with stoss-lee features. The stoss side was on the up-valley (southwest) side of the bedrock feature, and the lee side on the down-valley (northeast) side.

In general, WPII drift is thin and consists of erratics scattered on bedrock. However, drift forms thicker patches in two locations - on the south side of the central valley and on the valley walls. Clasts are composed of the local mafic and felsic banded gneissic bedrock, as well as some granite, granodiorite, diorite, gabbro, and mafic dike rock. The grain size is primarily sand to large cobbles, with a few regions additionally having small to moderate-sized boulders. Rocks are rounded to sub-rounded and have some light staining. A few erratics show moderate to heavy weathering; it is uncertain if these rocks were deposited already weathered as part of WPII drift or if they are from older deposits. Most exposed bedrock is strongly frost-shattered but remains nearly in situ, and thus can be defined as a felsenmeer surface.

2.2.3 Witalis Peak III Drift

Witalis Peak III (WPIII) drift extends in a nearly continuous sheet from the limit of WPII drift up the walls of the valley and onto the ridgelines. It is also visible in windows through WPII drift. Most of the northern ridge is draped by a sheet of WPIII drift, which also appears to extend down to Bowman Glacier. However, the northeastern end of this ridge displays areas of bedrock with little or no drift. WPIII drift also occurs in patches on the valley floor and extends to the southwestern ridgeline.

There are a number of morphological features associated with WPIII drift. On the northeastern valley wall, there are approximately 16 ice-marginal terraces (~30 m long) between ~410 and 460 m elevation. that rise in elevation from northeast to southwest. There are also at least six ridges (as much as 500 m long) on the northern valley wall that slope in the same direction. In addition, periglacial activity is evident across most of this deposit. There are regions where rocks have been reoriented by creep, sorted polygons, and perhaps even small stone stripes (Figure 13).

WPIII drift varies in color and composition, more so on the southern side of the valley, than on the northern side. Rocks consist of mafic and felsic components from the local gneissic bedrock, as well as granite, granodiorite, diorite, gabbro, and mafic dike rock. The grain size is primary sand to large cobbles, with a few small boulders. Rocks are moderately stained.

2.2.4 Radiocarbon Samples

We dated 17 samples of naturally freeze-dried ancient algae at the Witalis Peak field site (Figure 15; Table 1). These samples were collected primarily within sediment beneath small to large cobbles on strips of felsenmeer bedrock and amongst the thin WPII drift cover. The samples range from 0- 20 m elevation above the lake, and the dates range from 540 - 5510 years BP. The youngest date of 540 years BP is located immediately adjacent to the modern moat. Most samples dated to 1300-2800 years BP, with the exception of one, which yielded an age of 5510 years BP. We re-ran this sample and got an age of 4500 years BP. Given this uncertainty in age and the fact that it is significantly older than the other dates, we exclude this sample from further discussion at this time. The barium carbonate analysis of a water sample at this site yielded a modern age.

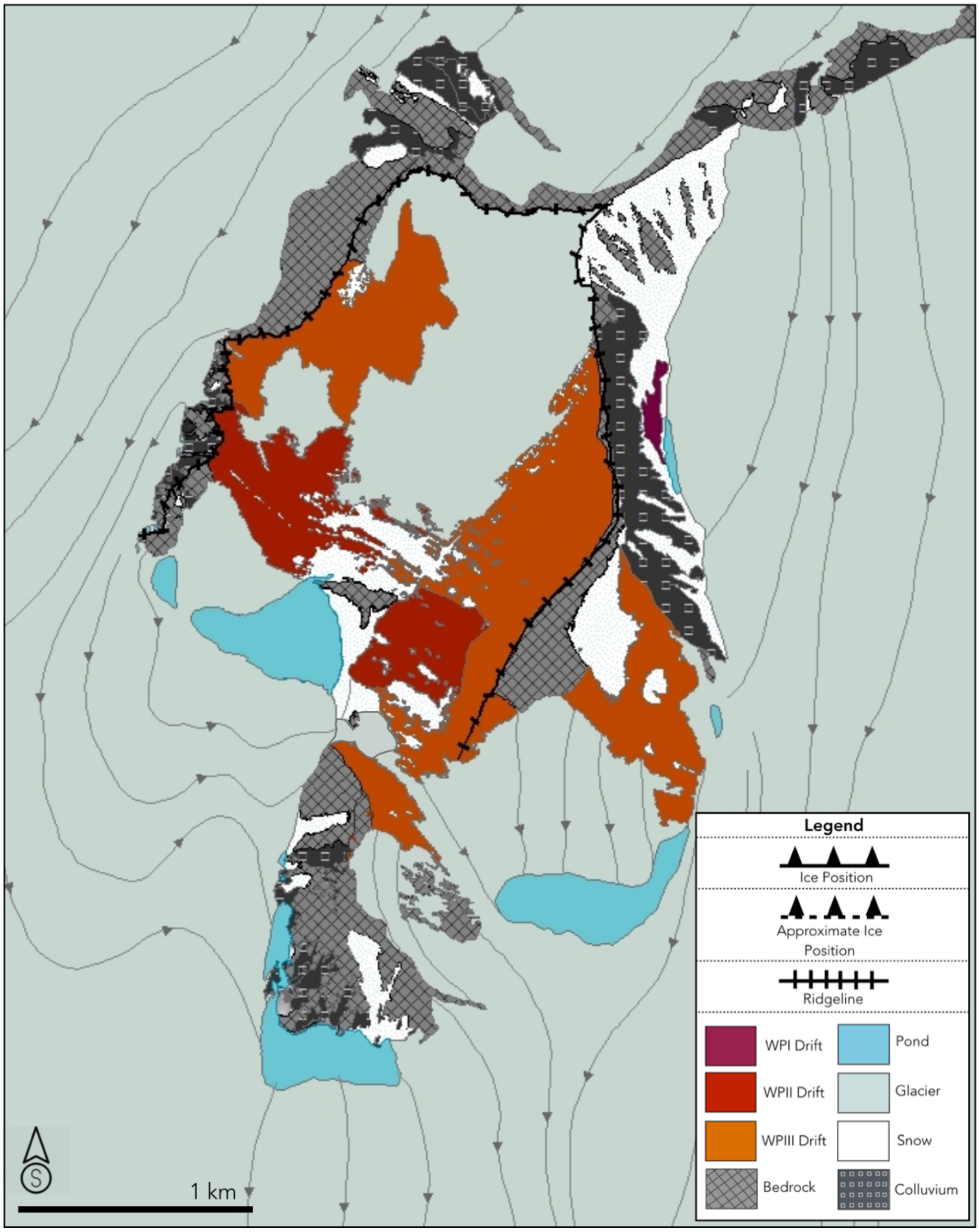

Figure 15. Witalis Peak map. Surficial geologic map based on field observations, using satellite imagery from the Polar Geospatial Center.

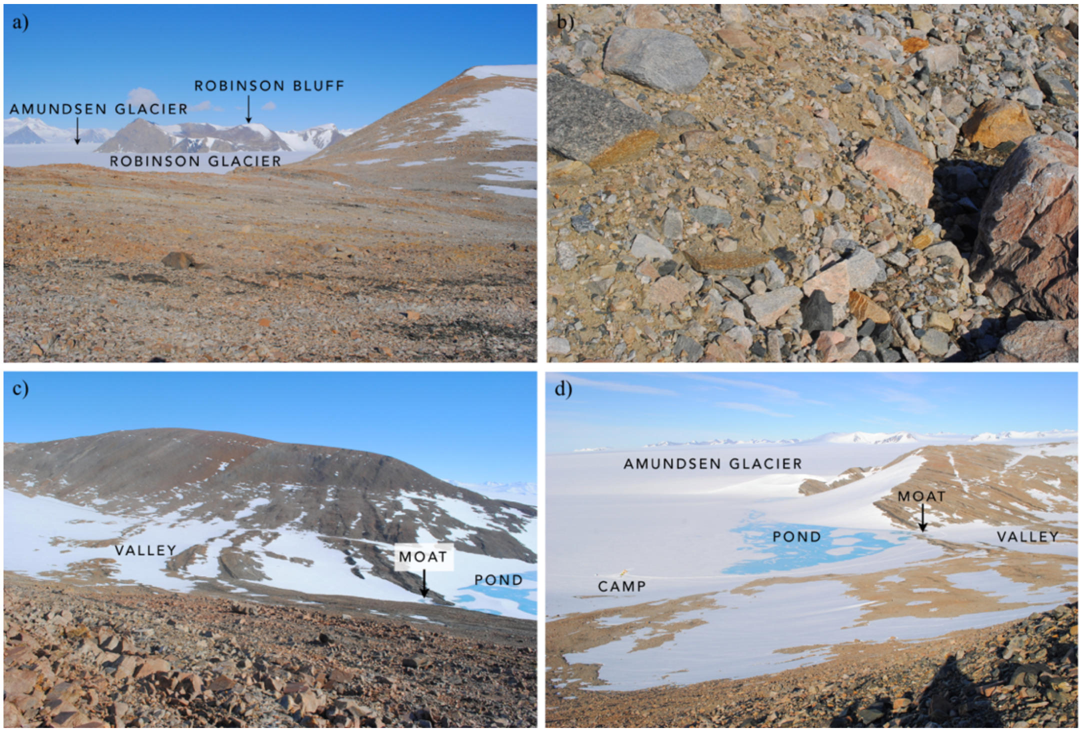

Figure 16. Witalis Peak photographs. a) The east ridge, WPII drift in the foreground, Robinson Bluff in the background. b) WPII drift showing the varied rock types and fine sediment fill. c) View of the central valley with vantage to the west from the east slope. d) View of the ice-dammed pond, with vantage to the southeast from the west ridgeline.

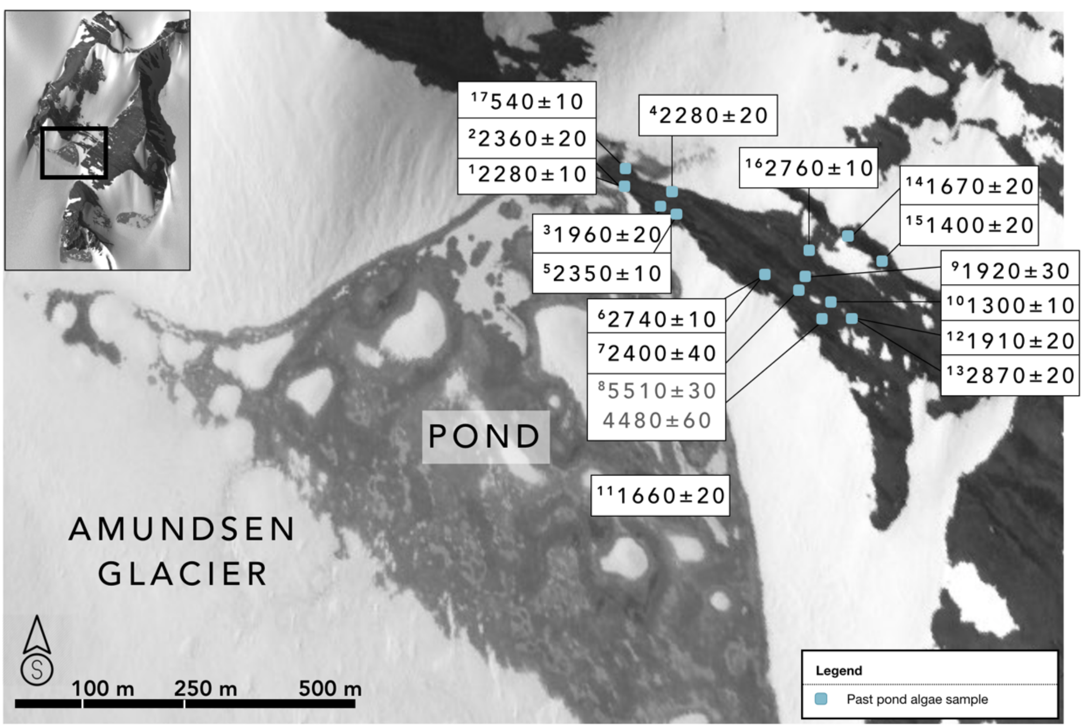

Figure 17. Radiocarbon dates at Witalis Peak. Numbers align with Table 1 and the outlier is labeled in grey.

Table 1. Dated Samples from Witalis Peak. Calendar year errors are 1 sigma. Probabilities less than 10% are not shown.

No.	Sample ID	Latitude	Longitude	Elevation (m)	^{14}C (yr BP)	^{14}C error	Probability	Calendar (yr BP)	Calendar error	$\delta^{13}C$
1	WP-16-4	-85.59214	-160.19176	282	2170	15	0.70	2280	10	-10.44
							0.30	2150		
2	WP-16-6	-85.59214	-160.19176	282	2380	20	0.65	2360	20	-6.63
							0.35	2410		
3	WP-16-7	-85.52921	-160.19646	284	1990	20	0.60	1960	20	-3.32
							0.20	1940		
							0.15	1980		
4	WP-16-8	-85.52924	-160.19746	284	2170	20	0.65	2280	20	-6.34
							0.35	2140		
5	WP-16-9	-85.52918	-160.19716	285	2360	20	1.00	2350	10	-8.04
6	WP-16-10	-85.52914	-160.20482	289	2580	20	1.00	2740	10	-6.29
7	WP-16-11	-85.52914	-160.20482	289	2410	20	0.95	2400	40	-3.51
8	WP-16-12	-85.52937	-160.20819	292	4780	25	0.90	5510	30	-8.23
							0.10	5580		
	WP-16-12_2	-85.52937	-160.20819	292	4010	60	0.95	4480	60	-7.09
9	WP-16-13	-85.52930	-160.20786	292	1970	25	1.00	1920	30	-3.6
10	WP-16-14	-85.52930	-160.21144	294	1390	20	1.00	1300	10	-2.51
11	WP-16-15	-85.52921	-160.21143	294	1750	15	0.50	1660	10	-2.35
							0.30	1630		
							0.20	1690		
12	WP-16-16	-85.52934	-160.21399	298	1960	20	1.00	1910	20	-2.01
13	WP-16-18	-85.52934	-160.21399	298	2780	25	0.70	2870	20	-4.14
							0.30	2910		
14	WP-16-20	-85.52977	-160.21031	292	1730	15	0.70	1670	20	-5.32
							0.30	1620		
15	WP-16-21	-85.52978	-160.21358	295	1530	15	0.80	1400	20	-5.7
							0.15	1510		
16	WP-16-25	-85.52922	-160.20212	287	2640	30	1.00	2760	10	-2.86
17	WP-16-26	-85.52921	-160.18909	281	550	15	0.90	540	10	-19.36
							0.10	620		
	WP-16-3	-85.52920	-160.19106	281	0	0	1.00	0	0	0

2.3 Surficial Deposits of Duncan Valley

I identified three distinct drifts at the Duncan Mountains field site, two of which extend inland and up valley from the present ice shelf, and one of which is on and adjacent to small local glaciers. Throughout much of Duncan Valley, there is evidence of re-working of deposits from reactivation and flow reversal of ice-cored debris and from periglacial activity. Because of the reworking, as well as the thin nature of one of the drifts, which is superimposed on the other deposit, it was difficult to determine the origin and relative age of some geomorphological features.

2.3.1 Duncan Mountains Alpine Drift

Duncan Mountains Alpine (DMA) drift occurs in two separate regions. I am correlating drifts at these sites based on the fact that both are lightly weathered and both are geomorphologically younger than the drift from the last glaciation.

DMA drift forms an ice-cored moraine fringing a local glacier that has advanced to push into the RIS. This glacier bounds part of the ice-dammed pond at the bottom of the valley and extends from the pond ~1.5 km to the east. DMA drift here consists of ~70% schist and ~30% granite, with rocks that range from rounded to angular and that are fresh to lightly weathered in appearance. The grain size ranges from gravel to medium boulders.

A second deposit of DMA drift occurs on the east side of Duncan Valley, where it forms a moraine deposited from a local glacier. This feature is about one kilometer long and parallels the glacier terminus. This drift, which is predominantly fresh to lightly weathered, consists primarily of schist, with some granite. Clasts range from round to angular. The grain size consists of small cobbles to large boulders, and the feature is unconsolidated with large void spaces. In many places, this deposit is composed of re-worked valley drifts, with molded and striated stones, indicative of Duncan Mountains III drift, present in many locations.

2.3.2 Duncan Mountains I Drift

Duncan Mountains I (DMI) drift extends on the valley floor adjacent to the ice-dammed pond (~ 47 m elevation) to ~760 m elevation, where it forms a clear drift limit marked by a one-meter-high bouldery moraine (Figure 16). In many places, this deposit is thin and is draped on top of the thicker, underlying Duncan Mountains II drift. As a result, the geomorphic features described below in association with this deposit may be composed of both drifts, and it is difficult in some cases to determine when the landform first developed.

Ice-marginal terraces are the most common landforms in Duncan Valley. Between the pond and ~100 m elevation, there are at least five small (~1-3 m high; ~60-100 m long) terraces. These are well preserved near the north valley wall and cross the valley, with their ice-contact side facing the ice shelf. Farther up-valley, the drift is very hummocky and broken up by frost cracks; there are sorted polygons in some locations. The hummocky nature of the drift makes it difficult to discern ~10 additional ridges and terraces within the central part of the valley.

Farther south, the valley splits into two arms. The southerly arm preserves approximately 15 terraces and 2 moraines. Some of these are prominent, whereas others appear to have been re-worked by slope movement, as indicated by their hummocky and discontinuous appearance. Their ice-contact sides appear to face down-valley. On the eastern slope above this valley, there are about seven additional moraines. These ridges step up to the DMI drift limit, which extends laterally across most of this slope for at least 550 m (Figure 16). The limit reaches ~760 m elevation and descends to the southeast. The northern arm of the valley displays hummocky ridges with as much as 20 m of relief. On the flat valley floor below the headwall, there are two small preserved ridges, each with an ice-contact side down-valley.

DMI drift consists of lightly weathered schist and granite with a sand and gravel matrix. Schist generally makes up most of the rocks (~70-80%), but in some areas the ratios are approximately equal. The rocks are angular to sub-angular, are primarily small cobbles to small boulders, and are lightly to moderately stained. Weathering increases up valley.

2.3.3 Duncan Mountains II Drift

Duncan Mountains II (DMII) drift extends from the valley mouth (~47 m elevation) to at least 807 m elevation. In most of the valley, it underlies DMI drift and is visible only in windows. The upper limit of the drift is unclear, as the deposit grades into local colluvium.

DMII drift appears to be very thick, as is evident by the prominent terraces (Figure 17) (~30 m high, 1-1.5 km long) positioned along the walls of the lower valley. Sections through these features show abundant amounts of glacial flour and till that contains molded and striated stones (Figure 17). Rock types consist primarily of schist and granite, as well as gneiss and pegmatite. The grain size ranges from silt to large boulders. The weathering of this deposit where it extends beyond DMI drift is moderate, with some staining.

2.3.4 Radiocarbon Samples

We dated 16 samples of ancient algae at Duncan Valley (Fig. 18, Table 2). Ages range from 880-4,180 yrs BP, and most are between 2,000-4,000 yrs BP. Although most samples relate to an ice-dammed pond in the valley, the sample collected at the highest elevation (134 m elevation) is associated with melt channels from the local glacier and thus does not bear on the history of the ice-dammed lake. The two youngest samples were collected near one another in the valley. Based on re-examination of the imagery and on my notes, it may be that these younger ages are the result of contamination from snow banks in this region, which could have resulted in melt pools not representative of the ice dammed-pond. Alternatively, lake levels could have been slightly higher than present as recently as ~1000 years ago. The barium carbonate analysis of a water sample at the ice-dammed pond yielded a modern age.

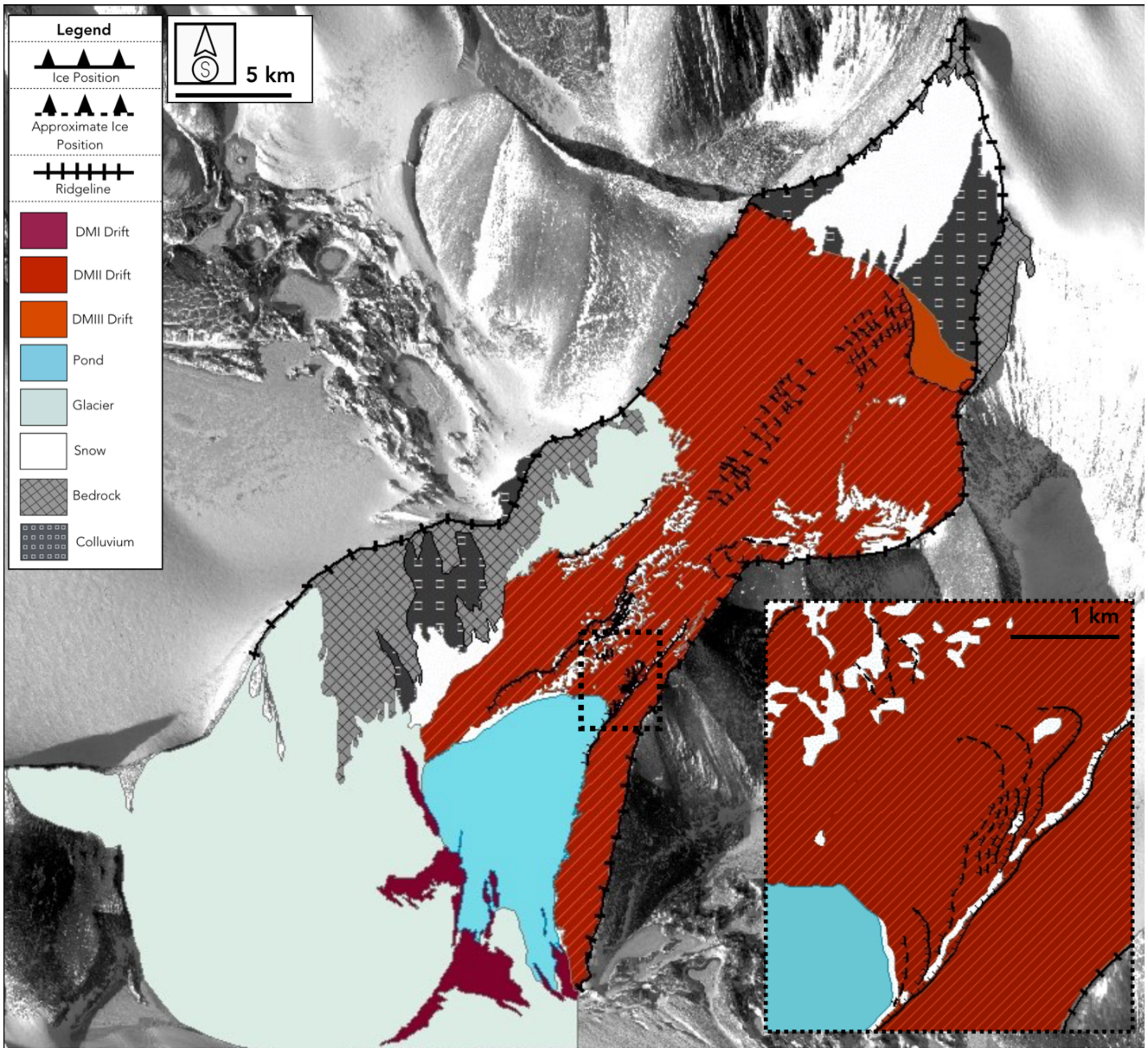

Figure 18. Duncan Valley map. Surficial geologic map based on field observations, using satellite imagery from the Polar Geospatial Center. Inset image shows the ice-marginal terraces where we collected most of our algae samples.

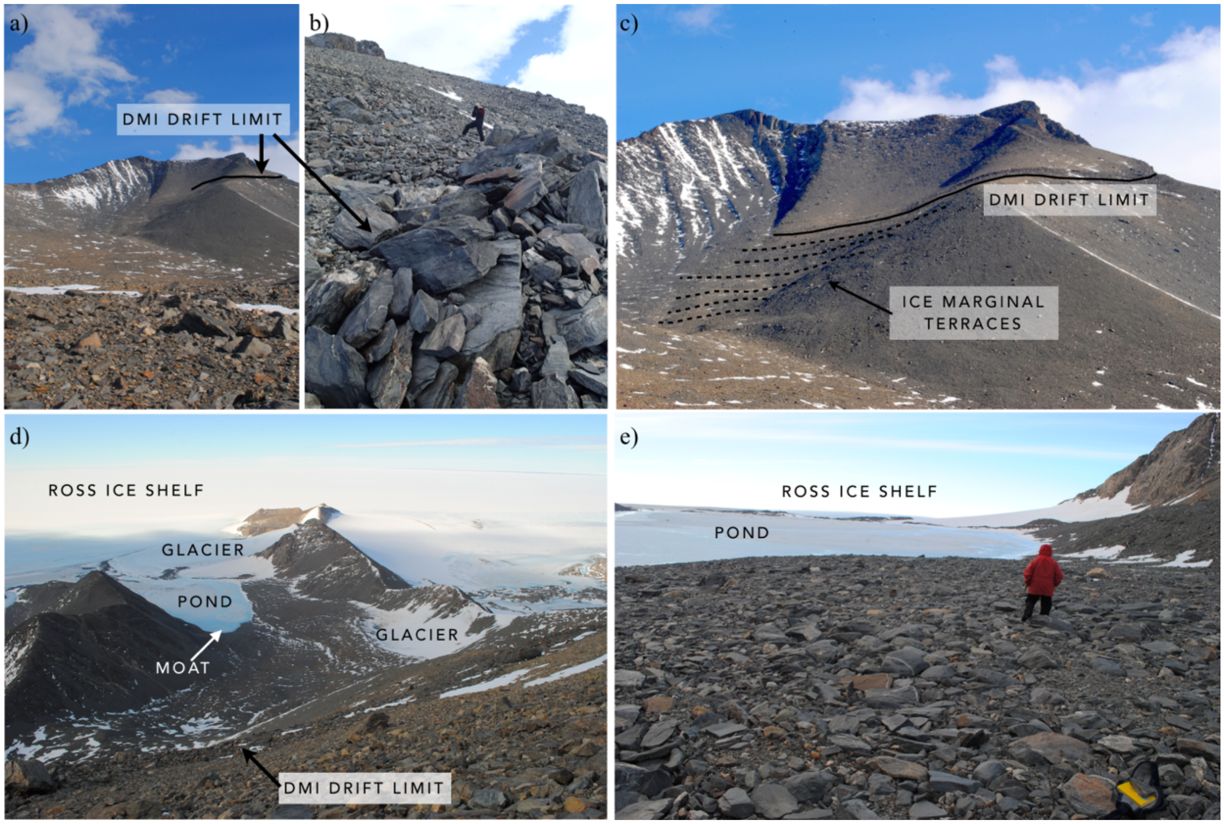

Figure 19. Duncan Valley photographs. a) View looking up valley towards the DMI drift limit at ~760 m. b) The moraine marking the DMI limit, with John Stone for scale. c) Ice-marginal terraces below the DMI drift limit. d) View looking down valley from DMII drift at ~800 m elevation. e) DMI drift overlying DMII drift at the bottom of the valley. This area appears to have been pressed into a pavement by the lake.

Figure 20. DMII drift. Images are of sections within the prominent terraces along the walls of the lower valley, which contain abundant amounts of glacial flour, as well as molded and striated stones.

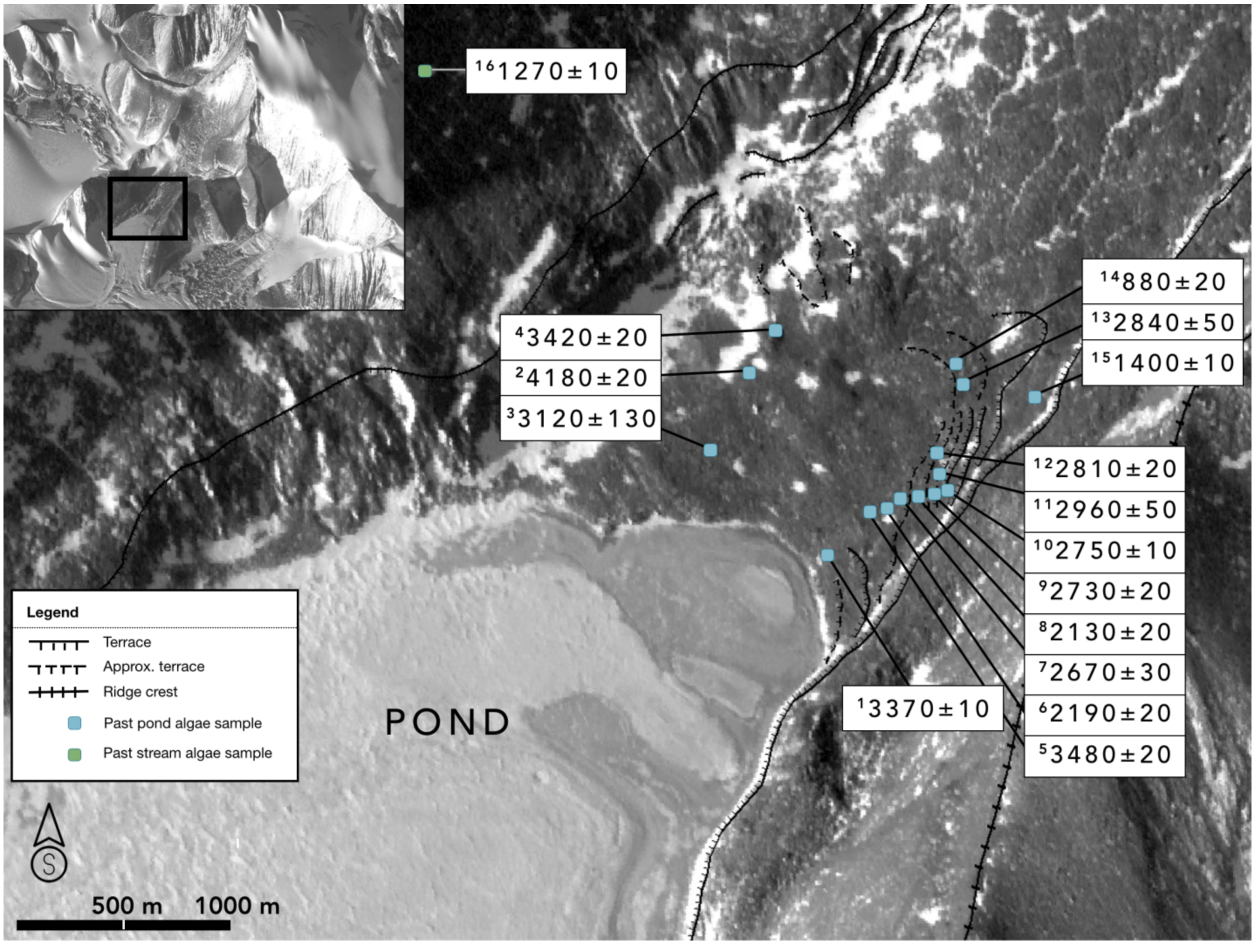

Figure 21. Radiocarbon dates at Duncan Valley. Numbers align with Table 2.

Table 2. Dated Samples from Duncan Valley. Calendar year errors are 1 sigma. Probabilities less than 10% are not shown.

No.	Sample ID	Latitude	Longitude	Elevation (m)	^{14}C (yr BP)	^{14}C error	Probability	Calendar (yr BP)	Calendar error	$\delta^{13}C$
1	DM-17-2	84.95679	166.48779	51	3150	15	1.00	3370	10	-17.52
2	DM-17-4	84.95775	166.47943	65	3830	15	0.70	4180	20	-8.45
							0.30	4230		
3	DM-17-5	84.95682	166.47403	52	2,970	95	1.00	3120	130	-15.52
4	DM-17-10	84.95823	166.47900	75	3210	20	0.80	3420	20	-5.32
							0.20	3440		
5	DM-17-18	84.95725	166.49089	57	3720	20	0.60	3480	20	-2.34
							0.40	3540		
6	DM-17-19	84.95728	166.49216	58	2220	15	0.40	2190	20	-5.57
							0.30	2230		
							0.15	2160		
7	DM-17-20	84.95737	166.49214	60	2470	15	0.50	2670	30	-4.51
							0.20	2600		
							0.20	2500		
8	DM-17-21	84.95741	166.49390	62	2130	15	0.80	2130	20	-5.03
							0.20	2070		
9	DM-17-22	84.95742	166.49457	64	2540	15	1.00	2730	10	-4.57
10	DM-17-23	84.95744	166.49586	66	2600	20	1.00	2750	10	-7.24
11	DM-17-24	84.95765	166.49651	67	2850	55	0.60	2960	50	-5.27
							0.20	2890		
							0.10	3020		
12	DM-17-25	84.95792	166.49568	74	2750	20	0.60	2810	20	-8.05
							0.40	2850		
13	DM-17-27	84.95825	166.49396	74	2760	50	0.90	2840	50	-6.91
14	DM-17-28	84.95824	166.49170	73	920	20	0.60	880	20	-7.61
							0.20	820		
							0.20	800		
15	DM-17-29	84.95894	166.50333	80	1540	20	0.40	1400	10	-18.84
							0.30	1500		
							0.30	1470		
16	DM-17-32	84.95884	166.44603	134	1300	15	0.60	1270	10	-3.12
							0.40	1190		
	DM-17-14	84.95621	166.47130	47	0	0	1.00	0	0	-18.53

2.4 Surficial Deposits of Mt. Mason

I identified two drift units at Mount Mason, one that extends across most of the nunatak and a more modern drift on the edge of the local glacier (Figure 19).

2.4.1 Mt. Mason I Drift

Mount Mason I (MMI) drift comprises the material currently on the local glaciers surrounding the northern side of Mt. Mason. This drift extends from the nunatak nearly seven kilometers northward across the Le Couteur Glacier. The drift is ice-cored and ranges from thinly scattered debris to moraines and distinct debris bands. The rock type is varied and includes 70-90% granite, as well as breccia, diorite, dolerite, basalt, gneiss, and meta-quartzite with mica.

2.4.2 Mt. Mason II Drift

Mount Mason II (MMII) drift extends across most of the nunatak, including throughout the main valley and on both ridgelines. While we did not explore the highest point of the mountain, the drift does appear to extend to peak (~816 m elevation). The drift displays numerous kettle ponds, especially within the central valley, as well as four moraines. Three of these trend approximately east-west for 0.4-1.2 km adjacent to the main ice-dammed pond (Figure 19). They have as much as six meters of relief on the ice-contact side and three meters on the ice-distal slope. We did not visit the fourth moraine, a gray, bouldery ridge, which occurs on the eastern valley wall.

MMII drift is a thick deposit with varied composition. The largest constituent is composed of a variety of granites (~70-90%). Other rocks include breccia, diorite, dolerite, basalt, gneiss, and meta-quartzite with mica. The rocks are sub-angular to rounded and exhibit light to moderate staining. Some rock types are heavily stained.

Figure 22. Mt. Mason photographs. a) MMII drift in the valley. b) View of the ridge separating the Le Couteur and Ross Sea basins. Vantage is to the southeast towards the valley and Mt. Mason. Note the different elevations of the two ponds. The ice-contact slope of a 0.5 m high moraine adjacent to the past pond basin is marked in black. c) View of the same ridge, with vantage to the north from the edge of the valley. d) MMII drift including a molded clast. e) A past pond basin with the ice-contact slope is marked in black.

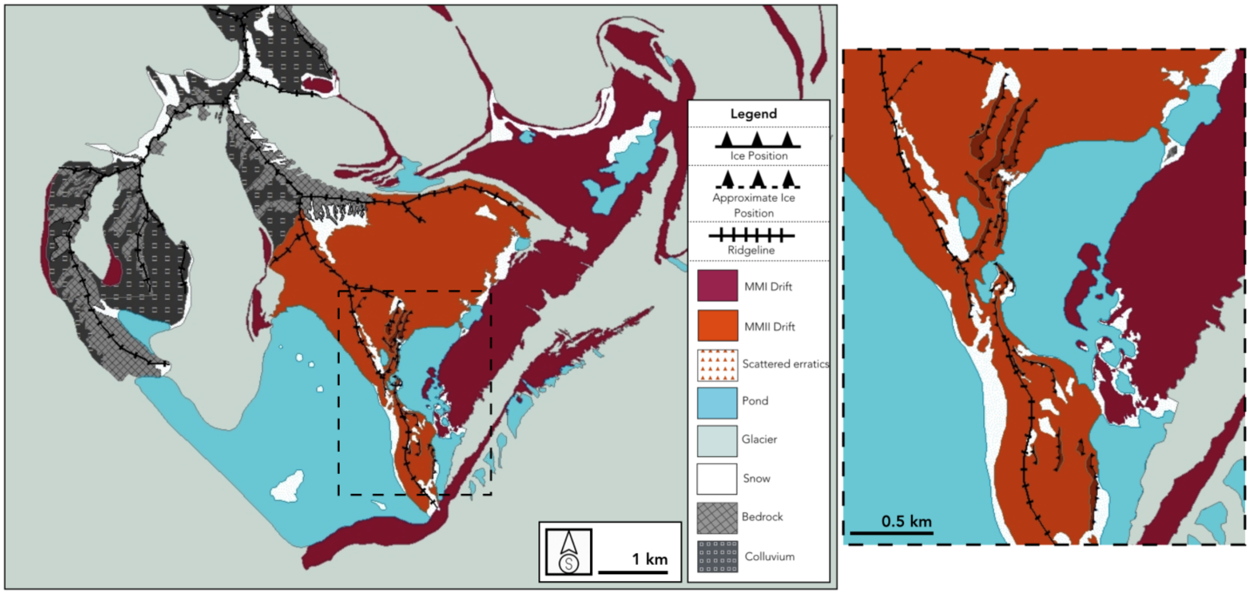

Figure 23. Mt. Mason map. Surficial geologic map based on field observations, using satellite imagery from the Polar Geospatial Center. Inset image shows moraines and ice-contact slopes extending from the valley to the northern end of the ridge.

2.4.3 Radiocarbon Samples

We dated nine samples of ancient algae at Mt. Mason (Figure 20, Table 2). Ages range from 1,490-3,120 yrs BP. The barium carbonate analysis of a water sample at this site yielded a modern age. These algae relate to two different ponds, which today are separated by a bedrock ridge (Figure 19). Some of our samples relate to slightly higher levels of the more inland of the two ponds. Others are from a time when ice-dammed water levels extended over the top of the bedrock ridge. In one location, a small moraine with an ice-contact slope facing northeast dams a small lake basin on the ridge crest (Figure 20).

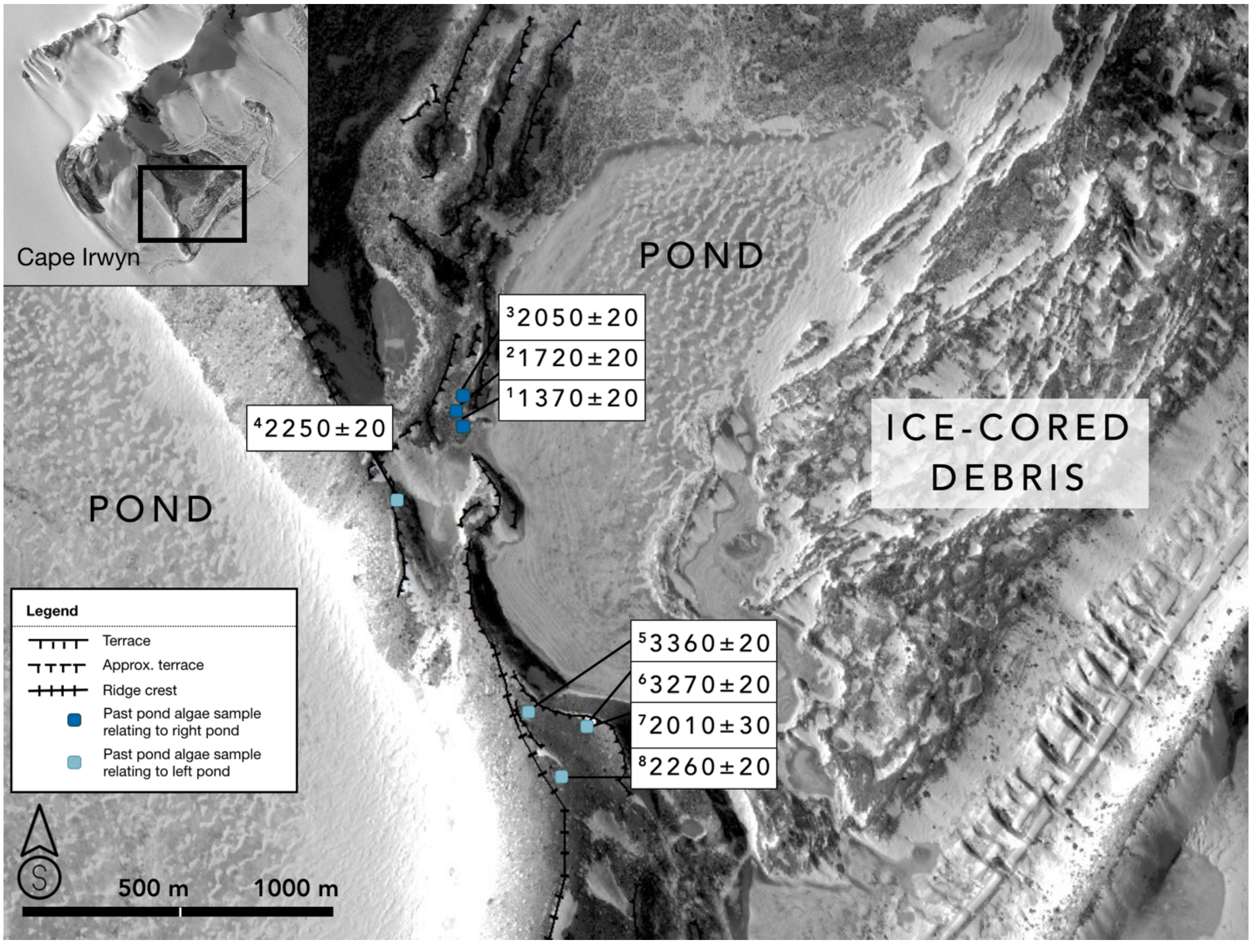

Figure 24. Radiocarbon dates at Mt. Mason. Numbers align with Table 3, and samples are color coded based on whether they are associated with levels of the left or right pond in the image. The left-hand pond is associated today with the Ross Ice Shelf and local ice off Mt. Mason. The right-hand pond is dammed by a lobe of Le Couteur Glacier.

Table 3. Dated Samples from Mt. Mason. Calendar year errors are 1 sigma. Probabilities less than 10% are not shown.

No.	Sample ID	Latitude	Longitude	Elevation (m)	^{14}C (yr BP)	^{14}C error	Probability	Calendar (yr BP)	Calendar error	$\delta^{13}C$
1	MM-17-2	84.69598	170.07866	224	1490	15	1.00	1370	20	-10.81
2	MM-17-4	84.69621	170.07744	227	1800	15	0.80	1720.5	20	-5.68
							0.20	1770		
3	MM-17-5	84.69630	170.07733	230	2090	20	0.40	2050	20	-6.36
							0.40	2090		
							0.20	2010		
4	MM-17-7	84.69483	170.06938	239	2210	20	0.40	2250	20	-5.96
							0.35	2170		
							0.15	2200		
							0.10	2300		
5	MM-17-9	84.69234	170.09462	249	3120	20	0.80	3360	20	-6.22
							0.20	3280		
6	MM-17-15	84.69214	170.10069	250	3090	20	0.60	3270	20	-7.47
							0.40	3340		
7	MM-17-16	84.69219	170.10051	250	2050	20	0.90	2010	30	-7.96
8	MM-17-17	84.69155	170.10242	254	2200	20	0.50	2260	20	-7.13
							0.35	2170		
							0.15	2290		
	MM-17-6	84.69598	170.07866	224	0	0	1.00	0	0	-15.93

2.5 Surficial Deposits of Mt. Henson

The surface of Mt. Henson appears very old (Figure 21b). The bedrock is broken into very stained felsenmeer, with more intact sections showing cavernous weathering. Erratics (here named Mt. Henson II drift) are sparse and heavily weathered and stained. Drift forming today on the local glacier (here named Mt. Henson I drift) adjacent to the north side of Mt. Henson extends a distance of more than four kilometers from the mountain and forms ice-cored moraines. In one location at the southern toe of Mt. Henson, in a wind scoop below the elevation of the modern ice, this drift was partially covering striated bedrock.

2.6 Surficial Deposits of the Tusk

I identified two drifts at the Tusk: modern deposits (here named Tusk I drift) of primarily granodiorite clasts forming hummocky moraines today on ice adjacent to the north to northwestern side of the Tusk and a thin older drift comprised mainly of lightly to heavily weathered and stained scattered erratics (Tusk II drift) on the ridgelines (Figure 25, 26). The surface of the Tusk itself appears very old, with heavily weathered marble bedrock (Figure 21c). Some areas display felsenmeer, and more intact sections show cavernous weathering. In contrast, the bedrock at low elevation (up to ~50 m) on the northeast ridgeline exhibits abundant deep striations (Figure 21d), which display several cross-cutting directions: 10°, 20°, 30°, and 60° (where 0° is set as north) at about 10 sites.

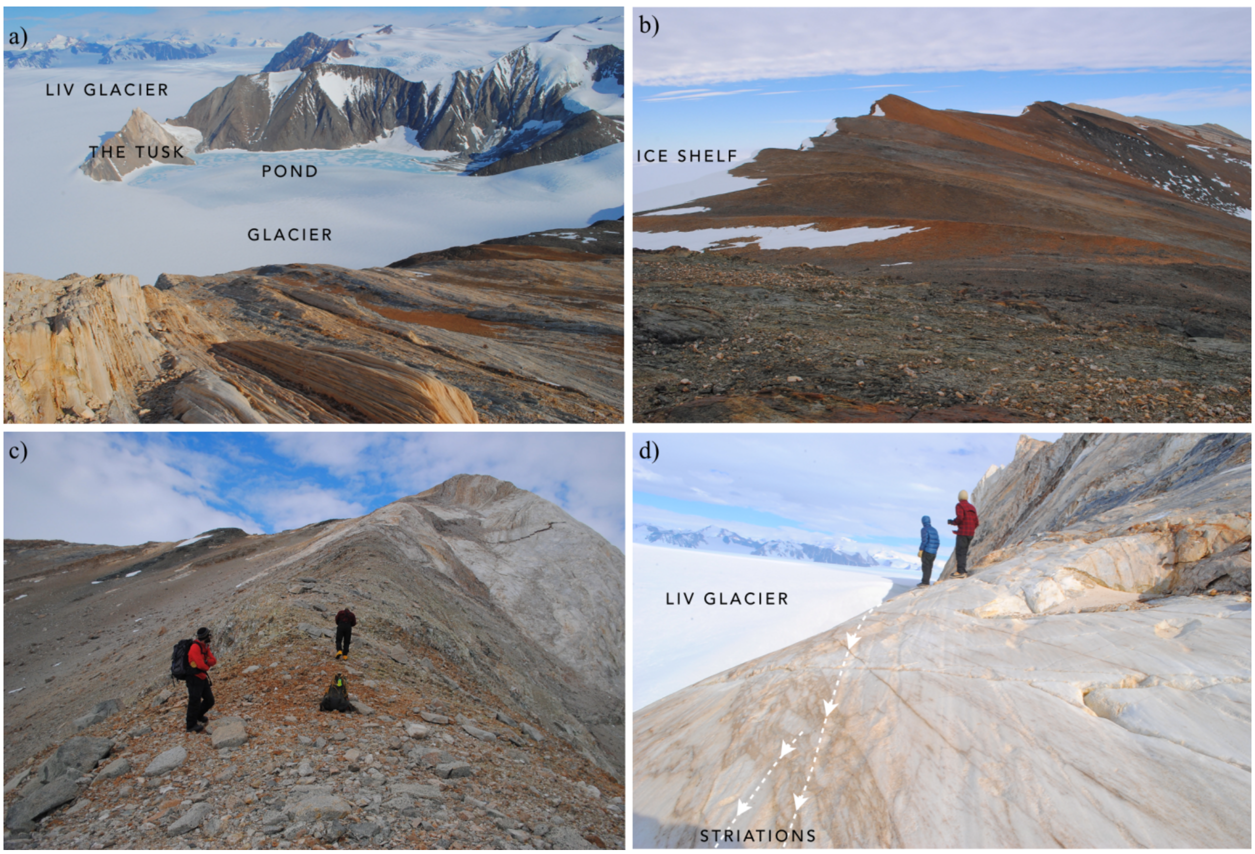

Figure 25. Mt. Henson and the Tusk photographs. a) Bedrock of Mt. Henson in the foreground, with view to the south toward the Tusk. b) Surface of Mt. Henson showing the highly weathered bedrock. c) West ridge of the Tusk, displaying scattered erratics (Tusk II drift). d) Striations on the lower Tusk on polished marble bedrock.

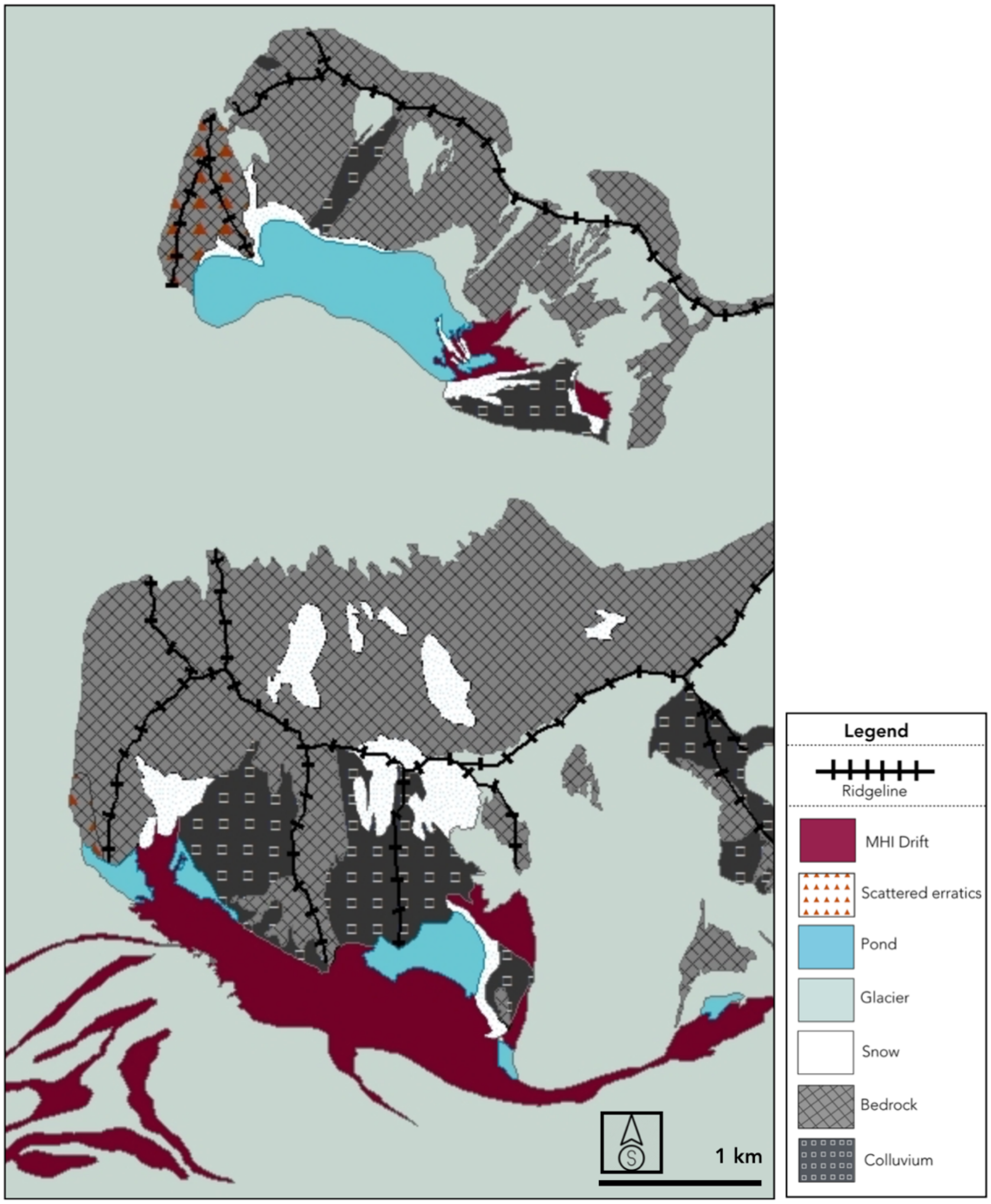

Figure 26. Mt. Henson and the Tusk map.

CHAPTER 3

INTERPRETATION OF GLACIAL DEPOSITS

3.1 Robinson Bluff

The drifts at Robinson Bluff were deposited by thickened ice from Amundsen, Robinson, and Whitney Glaciers (Figures 5a, 6a). Based on drift elevations and on the presence of erratics, at one time ice from these three glaciers covered the entire nunatak. When the ice became less extensive, it separated into lobes. Amundsen and Whitney Glaciers flowed against the south ridge of Robinson Bluff, Amundsen Glacier overtopped the east ridge, and Robinson Glacier flowed into the central valley. Both the relative weathering patterns and the geographic extent of these deposits suggest thinning ice over time. However, although weathering differences allow for a relative-age chronology, the amount of time represented by the deposits remains uncertain.

The lack of an absolute chronology allows two possible interpretations of the pattern and age of deposits at Robinson Bluff. The first hypothesis is that RBII-V drifts each represent a distinct glacial maximum, with the more extensive and more weathered deposits relating to older glaciations. If this is the case, then the drifts represent multiple glaciations, and ice level has decreased during each subsequent glaciation. By this scenario, Robinson Bluff would not have been covered entirely by ice during the LGM. Rather, the least weathered drift, RBII, would reflect an LGM limit at 600 m elevation, ~200 m above the present ice level. This hypothesis is favored by the strong weathering at high elevations on Robinson Bluff, consistent with a time span exceeding a single glacial cycle. Moreover, a pattern of consecutively older drifts at higher elevations is seen elsewhere in the TAM, such as at Hatherton and Reedy Glaciers (Bockheim et al., 1989; Bromley et al., 2010; King, 2017), and in these locations, the older drifts date to earlier glaciations. However, based on reconstructed LGM ice-surface elevations of ~1000 m elevation along the coast of the TAM both north and south of Amundsen Glacier (Bromley et al., 2010, 2012; Spector et al., 2017), it is likely that LGM ice elevations at Robinson Bluff would have been much higher than ~600 m elevation. Additionally, although rare, there are lightly weathered erratics on the ridge lines of Robinson Bluff to ~914 m elevation. If these erratics date to the LGM, they would indicate that the nunatak was completely covered in ice and that the RBII drift edge does not represent the LGM ice limit. This interpretation will be tested with surface exposure-age dating (Gombiner et al., in prep.).

The second possible interpretation is that RBII-V drifts were all deposited during the last glaciation and represent a continuum of drift laid down as the ice thinned during deglaciation. The extensive staining and exfoliation on the higher elevation deposits may still be compatible with this scenario, as weathering rates may be fast at this location due to the relatively warm and wet climate with extensive periglacial activity and running water (Figure 13). By this hypothesis, all of Robinson Bluff would have been covered by ice at the LGM.

There is another, less plausible hypothesis: that the more weathered drifts (all but RBII) are from prior glaciations and were preserved under cold-based ice at the LGM. Preservation of drifts is common in the TAM (e.g.,Bromley et al., 2010). However, at Robinson Bluff this hypothesis also would require that drift limits formed in the central valley at nearly the same elevation at some time during each deglaciation, even though ice may have reached higher elevations during the glacial maxima. Although unlikely, this may be possible if there is a threshold during deglaciation at which enough debris is available from newly exposed nunataks to allow for creation of drift sheets.

Although the exact interpretation of deposits at Robinson Bluff will remain unclear until absolute ages are obtained, I prefer a modified version of the second hypothesis - that most or all of the drifts at Robinson Bluff are from the LGM and subsequent deglaciation. I argue that the lower-elevation drifts (RBII-III) which form moraines date to the LGM, based on their weathering and well-preserved morphology. The higher-elevation drifts (RBIV-V), which underlie these are likely from prior glaciations, as they are very stained, are well-consolidated, and lack the well-preserved morphology of those downslope. They would have been overrun by cold-based ice during the LGM, which likely emplaced erratics as high as 914 m elevation.

3.2 Witalis Peak

The drifts at Witalis Peak were deposited by thickened ice from Amundsen, Robinson, and Bowman Glaciers (Figures 5b, 6a). Based on the elevation of the drifts and on the presence of erratics, ice from these three glaciers would have covered the entire nunatak at one time. The confluence of Amundsen and Robinson Glaciers flowed over Witalis Peak from the south and Bowman Glacier crossed the nunatak from the west. The presence and orientation of striations indicate that at one time, ice was channeled through the central valley.

I found fresh erratics (WPII drift) inferred to be from the most recent glaciation to at least 600 m elevation on Witalis Peak. Given that the peak reaches only ~623 m elevation, it is likely that the entire nunatak was covered by ice at the LGM. As the peak is well below the ice elevations (~1000 m) reconstructed from outlet glaciers to the north and south of this region (Bromley et al., 2012; Spector et al., 2017), the mountain probably was covered by several hundred meters of ice.

WPIII drift underlies and is distinctly more weathered than WPII drift. Because of these weathering differences I infer that WPIII drift predates the LGM. Subsequent areal scouring may have removed large areas of WPIII drift, giving it a patchy distribution, particularly on ridges near Amundsen Glacier.

3.3 Duncan Mountains

The areal extent of DMI drift suggests that it was deposited by ice along the Ross Sea coast (Figure 7b) that extended to a maximum observed limit of ~760 m elevation. Because DMI drift displays only light to moderate staining, I infer that it was deposited during the last glaciation.

The geometry of DMII drift is also consistent with deposition by grounded Ross Sea ice, in this case to a maximum limit of at least 807 m elevation. Based on a stronger degree of weathering than for DMI drift, I infer that DMII drift predates the LGM. In addition, based on the presence of numerous striated and molded stones (Figure 17), DMII drift may have been created under a wet-based ice regime, indicating different glaciological conditions from those that existed during deposition of DMI drift. This ice could have been thicker and/or flowed at a higher velocity than that which existed at the LGM, leading to basal sliding and subglacial erosion. However, fresh striations and polish on bedrock at sites adjacent to the coast suggest that even though DMI drift does not contain abundant striated and molded stones and rock flour, at least portions of the LGM ice sheet also were sliding. Another possibility is that DMII drift is composed of reworked Sirius Formation (Passchier, 2001), an older glacial deposit with abundant striated and molded stones.

3.4 Mount Mason

The drift at Mt. Mason was deposited by ice along the Ross Sea coast, as well as by Le Couteur and Morris Glaciers, both local glaciers (Figure 7c). Based on the extent and elevation of MMII drift, which extends to the peak (~816 m elevation), ice would have covered the entire nunatak. Further, the light to moderate staining on the clasts supports the hypothesis that MMII drift was likely deposited during the last glaciation.

Due to the complex ice dynamics at this site, it's difficult to interpret ice-flow directions during deglaciation. As the ice thinned, the topography (a bedrock ridge at ~250 m elevation) caused the glacier to separate into different lobes. To the west of the ridge that makes up Cape Irwyn, ice from Le Couteur Glacier receded from the valley in my field area. At the same time, grounded ice from the Ross Sea and the local Morris Glacier retreated from the east side of the ridge. Most of the moraines identified in the field area relate to the thinning and retreat of the Le Couteur lobe. However, a moraine banked up against the east side of the bedrock ridge, with an ice-contact side facing to the east, indicates that it was deposited by thicker Ross Sea ice. This moraine dammed a small pond on the top of the ridge in a bedrock-controlled depression.

3.5 Mount Henson and Tusk

The few erratics at Mt. Henson are all very weathered and thus do not afford direct evidence of ice cover during the last glaciation. However, given regional reconstructions, the mountain likely was covered mostly or fully by ice. The scarcity of fresh material may be due to the flow lines bringing relatively clean tributary ice rather than Liv Glacier ice over the mountain. The abundance of bedrock striations and polish on the lower Tusk and Mt. Henson indicate that the thickened Liv Glacier was sliding, at least at low elevations (Figure 21).

Scattered erratics (TI drift) at the Tusk display light to heavy staining and evidence of subaerial erosion, which may indicate that they reflect drift from several glaciations, with the youngest perhaps being from the LGM. Alternatively, all of the rocks may have been deposited during the LGM, but some of the heavily stained clasts may have been deposited already weathered.

The scarcity of deposits at Mt. Henson and the Tusk cannot be taken as reflecting a lack of LGM ice cover. Throughout the TAM, LGM deposits are commonly discontinuous, with some locations displaying extensive drift sheets and other sites exhibiting only rare erratics (e.g., at the mouth of Shackleton Glacier, Spector et al., 2017). This patchy coverage does not necessarily reflect the extent of ice cover, but is controlled primarily by flow directions, rock availability, and local sublimation-dominated ablation zones.

3.6 Alpine Glacier Deposits

Although not the primary focus of this study, I also mapped alpine glacier deposits in my field areas. These are best displayed in the Duncan Mountains, where a small alpine glacier has produced a distinct moraine composed of reworked DMI and II drifts. This relationship indicates that the alpine glacier advanced during and/or after retreat of Ross Sea ice from Duncan Valley and thus in the Holocene. Lower in the valley, another local alpine glacier has pushed into the Ross Ice Shelf, also suggesting recent advance. Evidence for re-advance of local glaciers at my field sites also occurs at Robinson Bluff and Mt. Mason (Figure 27). Advance of local alpine glaciers during the present interglacial also has been documented farther north in the McMurdo Sound region (Denton et al., 1989; Hall & Denton, 2000; Jackson, 2013; Stuiver et al., 1981), where it has been attributed to an increase in interglacial accumulation.

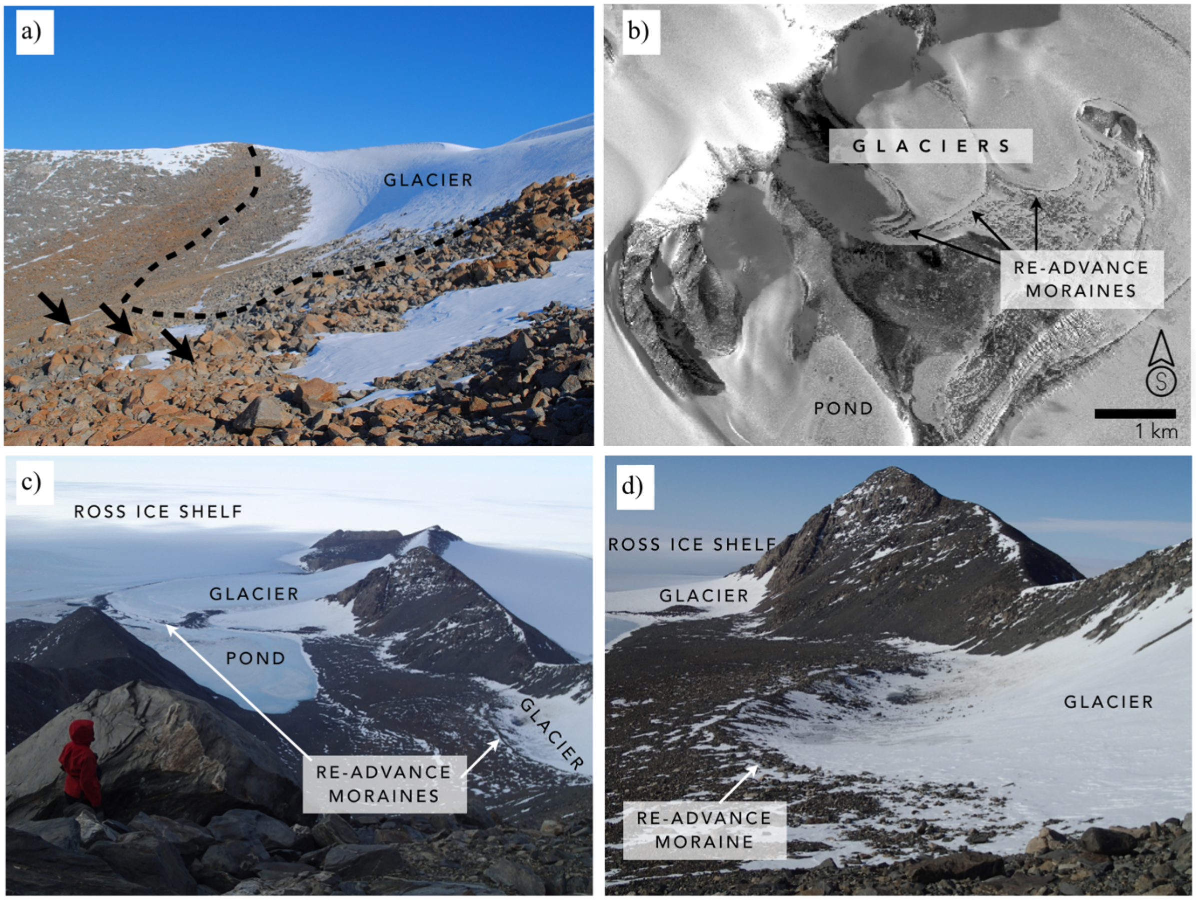

Figure 27. Alpine glacier deposits. a) View of a small alpine glacier at Robinson Bluff. The dashed black line denotes the limit of grey, less weathered drift recently covered by the glacier. The black arrows point to the presence of three left lateral moraines over the Undifferentiated Robinson Bluff drift. b) Alpine glaciers at Mt. Mason forming moraines where they push into the Le Couteur Glacier debris field. c) An alpine glacier in Duncan Valley on the right, and another alpine glacier extending between the pond and the RIS. Both glaciers have terminal moraine composed of re-worked DMI and DMII drifts, indicating their readvance. d) Small alpine glacier at Duncan Valley seen in (c), with its terminal moraine composed of reworked DMI and DMII drift.

3.7 Interpretation of Radiocarbon Ages

Radiocarbon ages of ancient algae provide information about the timing and nature of ice thinning at my field sites. The algae afford evidence for ponds that existed at elevations higher than at present. Because my samples are all located on slopes, ice would have been necessary to dam these ponds. Thus, the dates of algae afford information on the minimum elevations not only of the ponds, but also of the ice necessary to dam the ponds. In addition, the presence of algae also limits the maximum ice extent at that time and indicates that ice probably has not advanced beyond that location since the algae grew. Moreover, the oldest date of algae affords a minimum age for deglaciation of the site.

Previous work in the TAM has identified two primary scenarios for the evolution of ice-dammed ponds during deglaciation. The first is of continuous ice thinning and marginal retreat (Figure 28). Ice thinning down the sides of the nunataks results in downslope pond migration, following the glacier margin (Bockheim et al., 1989; Hall et al., 2016; King, 2017). Given this situation, I would expect the radiocarbon dates of algae to show a pattern of decreasing age with decreasing elevation. Moreover, because significant thinning at the mouths of outlet glaciers along the TAM coast precedes southward passage of the Ross Sea grounding line (Conway et al., 1999; Spector et al., 2017), one implication of scenario 1 is that the Ross Sea grounding line still remains north of the site.

In scenario 2, after an initial period of retreat, when most of the nunatak is deglaciated, ice thinning slows or stops, and the glacier reaches a stable position at or close to its present level (Figure 28). A period of stability or very slow thinning and adjustment results in an ice-dammed pond that covers approximately the same area, perhaps with some minor fluctuations due either to climate or small ice-marginal changes, for a long period of time. Given this situation, I would expect that the radiocarbon ages of algae would produce a range that encompasses the length of time that the pond (and ice) remained in more or less the same configuration. There would not be a consistent relationship between algae age and elevation. Moreover, the presence of the glacier at or near its modern elevation would be consistent with its terminus having reached floatation (i.e., part of the Ross Ice Shelf instead of a grounded ice sheet). Thus, in scenario 2, the Ross Sea grounding line already would have passed southward of the site.

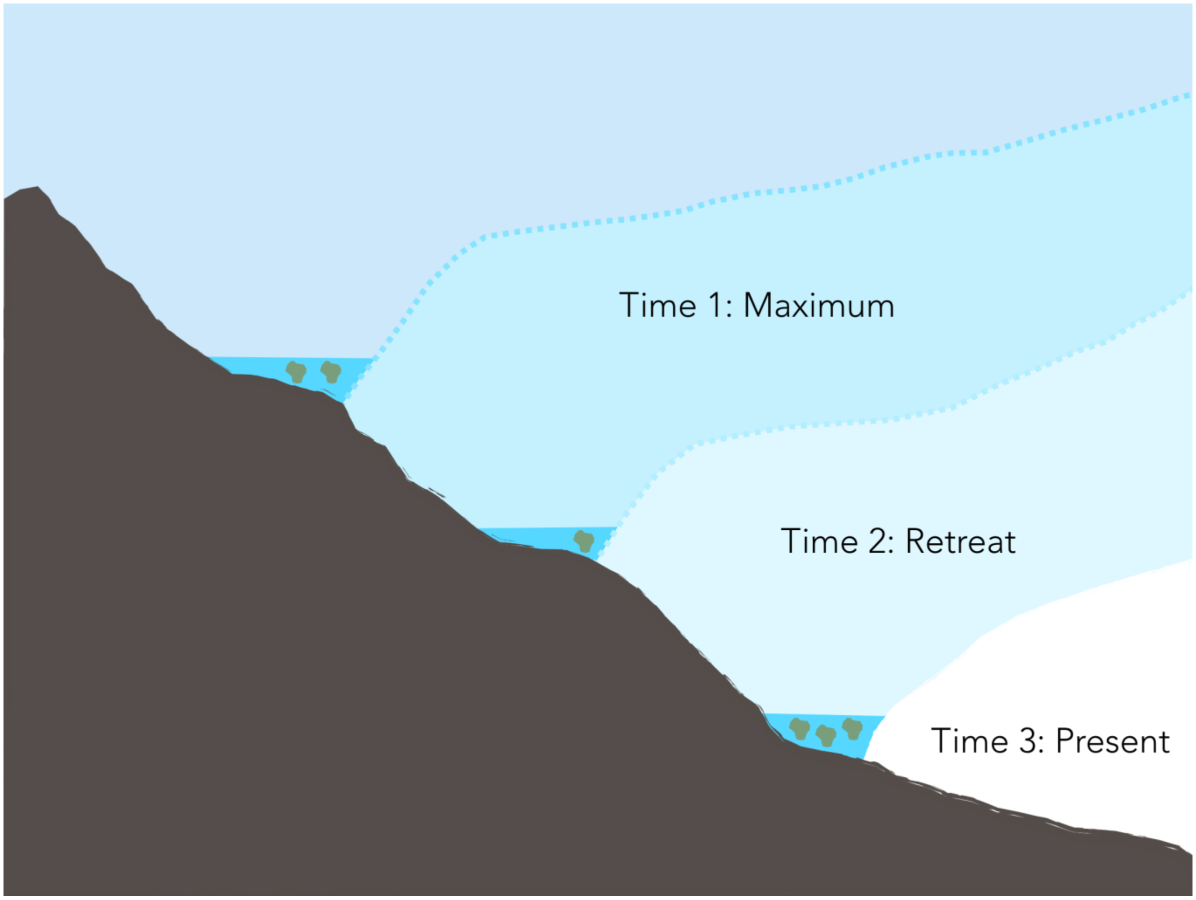

Figure 28. Scenario 1. Continuous ice thinning, with migration of the pond downslope, following the ice margin. Continuous thinning of the ice margin indicates that the glacier has not yet reached its present level at the floating ice shelf margin and thus the Ross Sea grounding line is still to the north of glacier terminus.

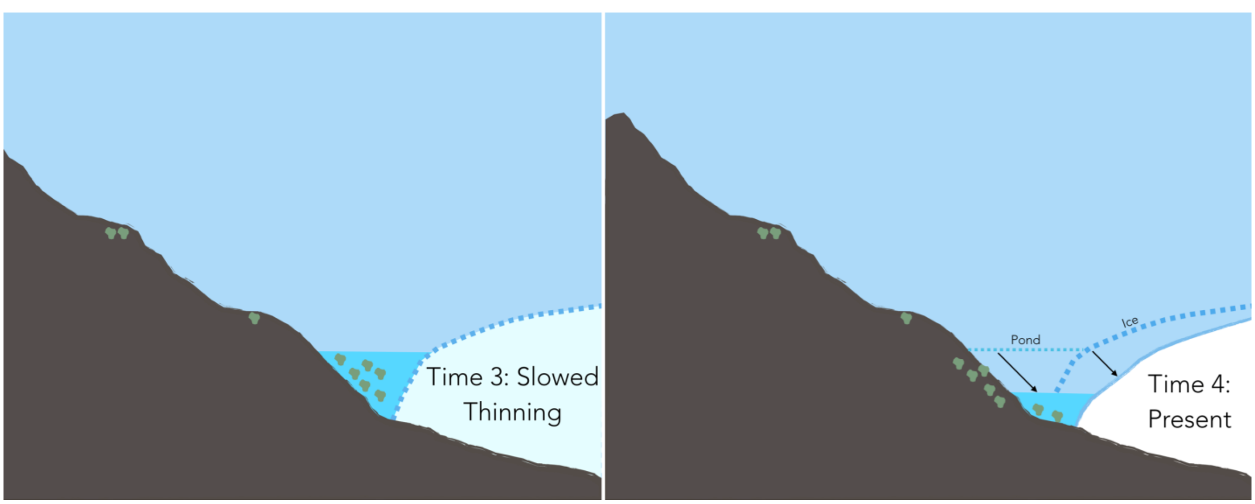

Figure 29. Scenario 2. Minor thinning or stability of ice close to its present level, indicating that the glacier likely has reached floatation at the level of the Ross Ice Shelf. In this instance, the Ross Sea grounding line has retreated south past glacier terminus and local ice is undergoing stagnation and readjustment.

Radiocarbon ages of algae collected at Witalis Peak afford several useful pieces of information. First, the oldest reliable age, 2,870 yrs BP, gives a minimum estimate for the timing of deglaciation. Amundsen Glacier must have been at or close to its present location by that time. Since then, the glacier has dammed a pond within 20 m elevation of its present level. There is no obvious pattern of age vs. elevation (Figure 30). Rather, the pond (and hence the glacier) appears to have occupied more or less a stable position for several thousand years. These data are consistent with Scenario 2 and further suggest that the Ross Sea grounding line passed this site by at least ~2900 yrs BP.

The algae samples collected in Duncan Valley indicate that ice once dammed the pond as much as ~40 m above its present elevation. The lack of ancient algae at higher elevations in the valley may be the result of deterioration under periglacial weathering, rather than a lack of a pond at a higher elevation during earlier stages of ice thinning. The highest-elevation sample was very fragile and disintegrated easily. Radiocarbon ages are as old as 4,180 yrs BP and indicate that deglaciation of Duncan Valley was nearly complete by ~4200 yr BP and that ice in the valley mouth was close to its present configuration. There is no relationship between algae age and elevation (Figure 30); the thinning that must have marked the early stages of deglaciation had been completed by 4200 yr BP. Rather, the geographic and temporal spread of ages supports the concept of a large pond filling this portion of the valley, at least periodically, for several thousand years, with ~40 m elevation of the present-day pond. These data again support Scenario 2 and suggest that the grounding line may have passed the Duncan Mountains by ~4200 yr BP.

Interpretation of the Mt. Mason data is more complex, given that results pertain to two different ice lobes with a constantly changing configuration of ponds. The more inland pond was dammed to as much as 20 m above its present elevation, whereas the seaward pond on the east side of the bedrock ridge was dammed as much as 50 m above present level. Thus, samples are linked to two different ice lobes with retreat in two directions. Some of the dates (1, 2, and 3 on the map) represent lowering of a pond dammed by Le Couteur Glacier and some (4-9 on the map) relate to thinning of coastal ice. The samples from the more coastal site show a range of ages, similar to those seen in the Duncan Mountains and at Witalis Peak. These may be consistent with a long-lived pond or series of ponds in more or less the same location. This implies that the grounding line had already passed Mt. Mason by the time of the oldest age, in this case, 3,360 yrs BP. In contrast, the samples that relate to a small pond fronting Le Couteur Glacier show a record of continuous drop in pond level, albeit only 20 m. This drop in water level may indicate that there has been minor thinning and adjustment of Le Couteur Glacier even once the Ross Sea ice became floating east in this region.

The radiocarbon data at my three field sites show several important similarities. First, there is no obvious linear relationship in the age vs. elevation profiles at any site, except for the three dates mentioned above by Le Couteur Glacier (Figure 30). Rather, each site affected directly by Ross Sea ice shows a spread of ages from samples all located at approximately the same elevation. Second, all of the dates fall within the late Holocene. At Witalis Peak, radiocarbon ages are all less than 2,870 yrs BP, and at the Duncan Mountains, less than 4,180 yrs BP. The ice and pond geometry at Mt. Mason is more complicated than at the other two sites, because of multiple ice lobes and ponds. Here, radiocarbon ages associated with the Ross Sea lobe span ~2,000 years between 1,370 and 3,360 yrs BP.

Based on these results, I conclude that the radiocarbon data produced in this study are most consistent with scenario 2, as outlined above. This observation favors the situation where ice thinning at Liv and Amundsen Glaciers was largely complete, and glacier termini had reached close to their present elevations at the ice shelf. The grounding line had passed southward of the field sites. If this is the case, then the oldest date at each site represents a minimum age for the timing of grounding-line retreat past each field sites. The oldest date yet obtained at the Duncan Mountains is 4,180 ± 20 yrs BP and at Mt. Mason is 3,360 ± 20 yrs BP. Coupled with the evidence for little change in pond or ice elevation in the last several thousand years, these dates thus suggest that the grounding line of the ice sheet had retreated past these sites at least by these respective dates. As Duncan Mountains is located south of Mt. Mason, I infer that the grounding line had retreated past the mouth of Liv Glacier by at least ~4,200 yrs BP. The oldest date at Witalis Peak is 2,870 ± 20 yrs BP and indicates that the grounding line had retreated past Amundsen Glacier by at least that time. I suspect that the retreat of the grounding line past these sites is unlikely to have been very much earlier, because I would expect to see older ages in the chronologies.

In summary, the radiocarbon chronology indicates the presence of long-lived ponds within a few tens of meters of present water level by at least 4,200 yr BP near Liv Glacier and 2,900 yr BP at Amundsen Glacier. These ages afford minimum-limiting constraints on the timing of grounding-line retreat past those glaciers (Figure 31). Assuming my dates closely constrain grounding-line retreat, ice recession in this sector of the Ross Embayment during the late Holocene was gradual, taking perhaps ~1,300 years to retreat the ~90 km from Liv Glacier to Amundsen Glacier.

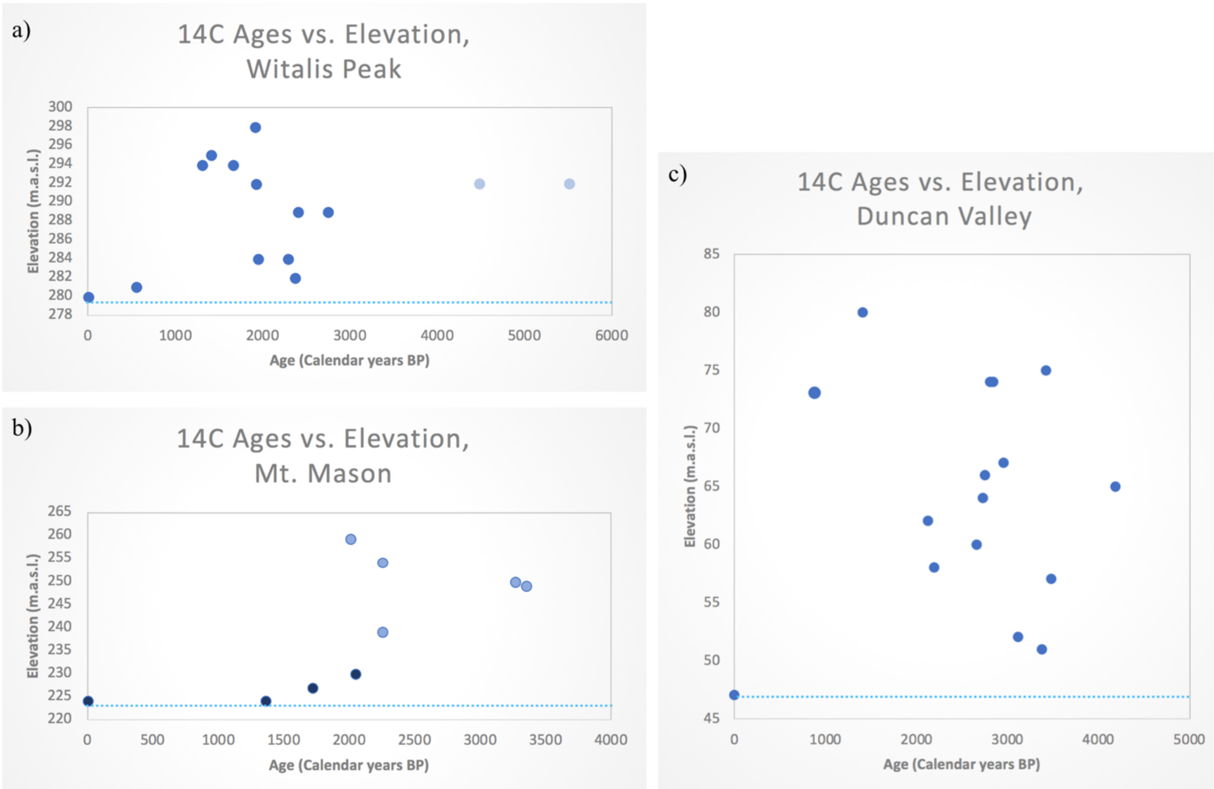

Figure 30. Age vs. elevation graphs. The dashed blue line represents the modern pond level at each site. a) Algae samples at Witalis Peak. Points in light blue represent two separate dates on one sample (number 8 in Table 1), inferred at present to be an outlier both because it is significantly older than other dates and because it is not reproducible. b) Algae samples at Mt. Mason. Dark blue dots represent samples pertaining to the lobe of ice damming the pond on the Le Couteur Glacier side (west) of the ridge and light blue dots represent samples pertaining to the lobe of damming the pond on the Ross Sea side (east)(Figure 24). c) Algae samples at Duncan Valley.

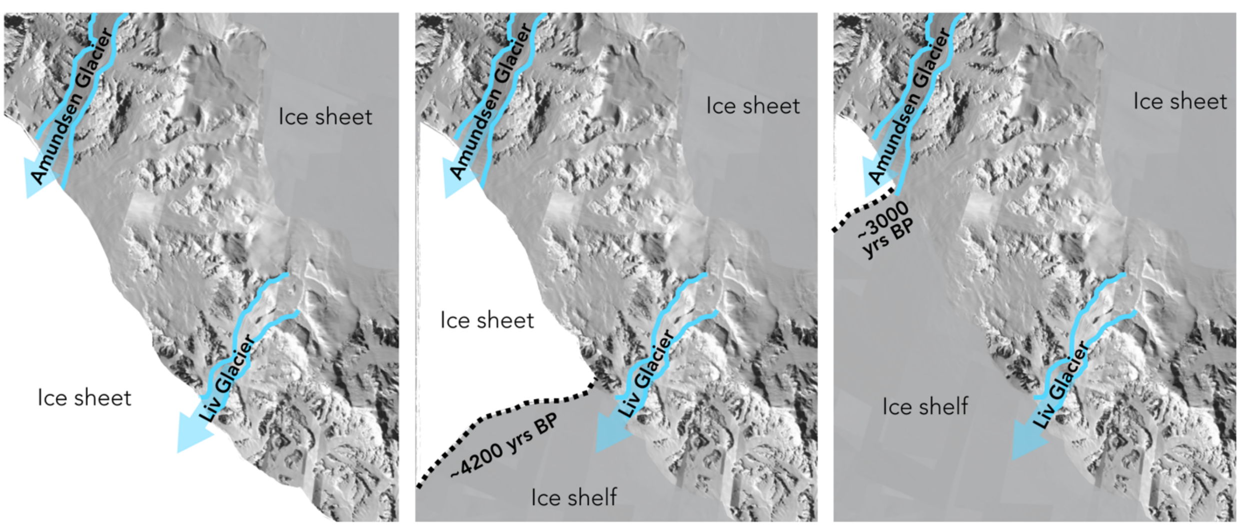

Figure 31. Grounding-line retreat illustration. This figure shows the approximate retreat of the ice sheet in the southern Ross Embayment. In the left box the ice sheet is grounded in the Ross Sea north of the field areas. In the middle panel, the ice sheet has retreated past Liv Glacier by ~4,200 yrs BP, and in the right box the ice sheet has retreated past Amundsen Glacier by ~3,000 yrs BP.

CHAPTER 4

COMPARISON TO OTHER ANTARCTIC RECORDS

4.1 Timing of Deglaciation in the Southern TAM

Geologic data from the TAM suggest that initial thinning of ice in the Ross Sea sector occurred at ~13,000 yrs BP (Hall et al., 2013). Geologic evidence in support of this timing is seen along the Scott Coast (Hall & Denton, 2000), in the Royal Society Range (Hall et al., 2015; Jackson et al., 2017), at Beardmore and Scott Glaciers (Spector et al., 2017), and as far as the southernmost outlet glacier in the TAM, Reedy Glacier (Todd et al., 2010). These latter three outlet glaciers feed the former flow lines in the central Ross Sea, whereas the other sites mentioned are adjacent to the western Ross Sea. The timing of recession in both the western and central Ross Sea is similar to that recorded in the eastern Ross Embayment. Some interpretations of glaciological data suggest that Siple Dome thinned between 15,000 and 10,000 yrs BP, and models show that ice-stream thinning may have been underway by ~13,000 yrs BP along the Siple Coast (Parizek et al., 2003; Price et al., 2007).

Existing glacial geologic and relative sea-level data point to a massive retreat of the grounding line (as much as ~1,000 km) between 9,000-7,500 yrs BP in the Ross Embayment. Relative sea-level curves along the Victoria Land Coast, determined from ^{14}C dates of preserved penguins, seals, shells, and seaweed in raised beaches, provide a timing of final ice-unloading (Hall et al., 2004). These results indicate final unloading of the ice sheet just before 8,200 yrs BP in Terra Nova Bay (Baroni & Hall, 2004), and ~7,800 yrs BP farther south along the Scott Coast, inland of Ross Island (Hall et al., 2004). McKay et al., (2016) interpreted planktonic and benthic foraminifera in a marine core to the east of Ross Island as an indication of open-water conditions. Benthic foraminifera produced an age of ~8,600 yrs BP, which led McKay et al. (2016) to conclude that the grounding line had retreated east of Ross Island by this time, a few hundred years earlier than relative sea-level dates from the Scott Coast. In a study at Mackay Glacier also along the Scott Coast, Jones et al. (2015) sampled erratic cobbles along transects at two nunataks (~7 and 14 km from the coast). Exposure ages tied to glaciological models were used to investigate changes in glacier surface elevation. Together, both lines of evidence suggest that rapid thinning occurred at ~7,000 yrs BP (Jones et al., 2015). In the central TAM, exposure ages show that ice just offshore of Beardmore Glacier came afloat at ~7,800 yrs BP (Spector et al., 2017). Rapid ice thinning , possibly corresponding to grounding-line retreat near Beardmore Glacier, is recorded between ~8,400-6,300 yrs BP much farther south on Mt. Rigby at Scott Glacier (Spector et al., 2017). Taken together, these studies suggest that a large sector of the Ross Sea from Terra Nova Bay to at least as far south as Beardmore Glacier experienced widespread grounding-line retreat at ~9,000-7,500 yrs BP.

This rapid grounding-line recession may have extended as far south as Shackleton Glacier, only 100 km north of the Duncan Mountains field site near Liv Glacier. Limited and incomplete information from surface exposure ages 50 m above the ice at Gemini Nunataks (25 km up-glacier of the Ross Sea coast) suggests that Shackleton Glacier may have been nearing its present-day level by 7,700 yrs BP (Spector et al., 2017). Although interpretation of these data is hampered by the fact that they are not situated on the coast, it appears that the grounding line may have retreated as far south as Shackleton Glacier not long after reaching Beardmore Glacier.

Interpretations from my field sites help to document grounding-line retreat in the second half of the Holocene in the region southeast of Beardmore Glacier. Radiocarbon chronologies suggest that the grounding line retreated past Liv Glacier by at least ~4,200 yrs BP, and past

Amundsen Glacier by at least ~2,900 yrs BP. Although my data afford only minimum-limiting age constraints, it seems likely that had the grounding line passed my field sites significantly before these times, I would have found evidence of lakes dating to that earlier time period. I did not find such lakes nor any evidence that ice was near present-day level as early as ~8,000 yrs BP. Thus, I infer that the grounding line probably remained north Liv Glacier during the event that caused massive deglaciation at 7,500-9,000 yrs BP. Confirmation of this hypothesis awaits surface exposure-age dating of erratics, which is underway at the University of Washington. However, data from Scott Glacier afford circumstantial evidence in support of my estimates, at least at Amundsen Glacier. Given the proximity of Scott and Amundsen Glaciers (35 km apart), one would expect them to show similar timing for grounding-line recession. From an erratic perched on bedrock close to present ice level, Spector et al., (2017) concluded that the grounding line may have reached Scott Glacier shortly after 3,400 yrs BP, which is close to my estimate of shortly before 2,900 yrs BP at Amundsen Glacier. Because the present grounding-line is just south of the mouth of Scott Glacier, these two pieces of evidence together indicate that ice had reached its present position by ~3000 yrs BP.

Assuming my data accurately reflect the timing of grounding-line retreat, and recession did not proceed to Liv Glacier until just before 4,200 yrs BP, there appears to have been a change in the rate of recession sometime after ~7,800 yrs BP south of Beardmore and possibly Shackleton Glacier. Calculation of the precise rates of grounding-line retreat at different times is hampered by uncertainties in the exact direction of recession. Recession along the TAM coast between ~8,200 and ~7,800 yrs BP ('swinging-gate' model of Conway et al., 1999) would have occurred at a rate of ~2.4 km/yr if it proceeded in a north-south direction from Terra Nova Bay to Beardmore Glacier. Calculations of grounding-line retreat become more speculative if, as is likely, ice recession started in the center of the Ross Sea and proceeded both southward and toward the coast ('saloon doors' model of Ackert, 2008). An estimate of grounding-line position at 9,000 yrs BP at approximately the present-day RIS front in the central Ross Sea yields an average rate of recession to Beardmore Glacier of ~0.5 km/yr. In contrast, my data suggest that the grounding line may have receded at a rate of only ~0.1 km/yr from Duncan Valley to Mt. Rigby at Scott Glacier. Possible causes for this proposed change in the retreat rate are discussed in Section 4.2.

4.2 Forcing Mechanisms

In order to evaluate hypotheses about past and potential future behavior of an ice sheet, it's important to consider and understand the physical processes that affect its components. A body of ice ultimately is governed by its mass balance, determined by net thinning and thickening across its areal extent. Hughes (2009) argued that ice sheets have stable interiors which constitute ~90% of the ice volume, and that these have overall passive responses to external forcing. However, the periphery of an ice sheet may be unstable, because it contains energetic components, particularly ice streams. Ice-stream motion is affected strongly by ice-bed coupling, which can vary over time in response to climate, sea level, ice accumulation and ablation at the surface, erosion/deposition at the bed, subglacial hydrology, sinking and rebound of the land, and ocean-atmosphere heat transport. The height of an ice sheet above its bed is primarily based upon climatic factors, as well as on the strength of this coupling. Uncoupling, which mainly occurs along the periphery, particularly in ice streams, reduces ice height by as much as 90%, with another ~9% of lowering occurring in the extension of ice into a floating shelf (Hughes, 2009), and can lead to a strongly negative mass balance.

Recent glaciological studies show that ice streams that drain the interior of the WAIS and feed the eastern RIS have a dynamic nature and can change their flow directions on short (at least century) time scales (Conway et al., 2002). These ice streams have significant wet-based portions and their basal conditions, including melt rates and till thicknesses, can cause fast flow. As a result, the ice streams can alternate between periods of activity and stagnation (Conway et al., 2002; Fahnestock et al., 2000; Hulbe & Fahnestock, 2007). In contrast, the outlet glaciers feeding the western side of the RIS draining the EAIS do not display periods of stagnation and acceleration, as their beds are largely frozen and resting on bedrock. However, some studies suggest that EAIS outlet glaciers have high driving stresses due to their thicknesses, and as a result, may be more sensitive to changes in buttressing from the RIS (Stearns, 2011; Stearns & Hamilton, 2005).

Examination of ice-sheet history can help determine what controls ice-sheet behavior on longer time scales. The studies in Section 4.1 show that the emerging story in the Ross Embayment is one of a late LGM, the time of which varies geographically. Significant deglaciation was delayed until after 13,000 yrs BP, and most-grounding line recession occurred in Holocene time (Allard et al., 2013; Anderson et al., 2014; Conway et al., 1999; Hall et al., 2013, 2015; Jackson et al., 2017). Following rapid retreat between ~9,000-7,800 yrs BP, there was a transition to much slower retreat in the second half of the Holocene, which suggests that the ice sheet may have been close to re-stabilizing.

An important question with implications for understanding future ice-sheet stability is why the retreat of the AIS in the Ross Sea sector was delayed relative to the global deglaciation. The majority of atmospheric and oceanic warming, as well as sea-level rise, which marked the end of the LGM, all occurred well before most thinning and grounding-line retreat of the ice sheet in this region (Braddock, 2014; Fairbanks, 1989; Kim et al., 2012; Koutnik et al., 2016; Masson et al., 2000). Moreover, glaciers in the southern mid-latitudes were nearly at Holocene positions by the time deglaciation got underway in the Ross Embayment (Clapperton & Sugden, 1988; Heirman et al., 2011; Putnam et al., 2013; Putnam & Schaefer, 2013).

The global and local forcing mechanisms that are most important to consider in addressing the cause of AIS retreat are accumulation rate, ocean temperature, and sea-level change, both global and local. Atmospheric temperature is not a crucial parameter, as ablation in the Antarctic is almost entirely from sublimation rather than from melting (Bliss et al., 2011), and the increase in temperature allows more precipitation to occur (Hall et al., 2015; Simpson, 1934). In order to be considered a valid possible forcing mechanism, each of these potential forcing parameters must be consistent with the following glacial history: 1) deglaciation delayed largely until the Holocene; 2) subsequent rapid retreat between ~9,000-7,800 yrs BP; and 3) slowing retreat sometime after 7,800 yrs BP, with gradual recession between ~4,000-3,000 yrs BP. To assess how successfully each parameter can explain the glacial history, I'll first discuss the potential forcing mechanisms (Table 4), and then show how these factors may have influenced ice-sheet behavior.

Increased accumulation during the present interglacial may have delayed deglaciation (Hall et al., 2015). Records from the WAIS Divide Ice Core show a doubling of snow accumulation over West Antarctica after the time of the global LGM (WAIS Divide Project Members, 2013). The level of accumulation remained high throughout the Holocene, especially between ~9,200-2,300 yrs BP (Koutnik et al., 2016). The persistence of a high accumulation rate during the Holocene is also recorded by re-advances of independent alpine glaciers, from the Dry Valleys (Denton et al., 1989) to my field sites in the southern TAM. High accumulation is thought to have caused a delay in the timing of the maximum in Antarctica, particularly at inland sites along the TAM from Hatherton Glacier to Reedy Glacier (Hall et al., 2015; King, 2017; Todd et al., 2010). Eventual thinning of the ice sheet and subsequent grounding-line retreat in the Ross Sea indicate that while accumulation may have partially slowed retreat, it did not stop it. This suggests that some other mechanism overwhelmed the accumulation effect, at least in areas affected by marine influence (Hall et al., 2015). However, the continued increase in accumulation throughout most of the Holocene could have played a role in the slowing of grounding-line retreat after 7,800 yrs BP. The maximum Holocene accumulation rate occurred between 4,000 and 2,000 yrs BP (Koutnik et al., 2016) and appears to correlate in time with the slow grounding-line recession seen between Liv and Scott Glaciers.

Warm ocean temperatures have been implicated in present and past grounding-line retreat (Kimura et al., 2016; Pollard et al., 2015; Shepherd et al., 2004) and could have played a role in Antarctic deglaciation. This linkage is seen today at WAIS outlet glaciers in the Amundsen Sea sector, where warm Circum-Polar Deep Water (CPDW) reaches the grounding line and is thought to be responsible for rapid recession (Dutrieux et al., 2014; Joughin et al., 2014b; Rignot et al., 2014). Access of warm water masses to particular portions of the floating ice tongue or ice-sheet grounding line may be very important for stability. For example, at Pine Island Glacier melting is delayed by a sea-floor ridge that blocks the warmest CPDW from reaching the thicker ice at the grounding line of the floating ice tongue (Dutrieux et al., 2014). In the Amundsen Sea region, the shift to greater CPDW flow and glacial melt has been a result of increased westerly wind stress near the Antarctic continental shelf (Steig et al., 2012).

Temperatures in the Southern Ocean began to increase by ~17,000 yrs BP (Anderson et al., 2009; Denton et al., 2010). This increase was punctuated by a cooling referred to as the

Antarctic Cold Reversal (~14,500-12,900 yrs BP), after which temperatures again began to rise, peaking at ~12,000 yrs BP before gradually decreasing throughout the Holocene (Crosta et al., 2004). In the Ross Sea region, there is a scarcity of reliable ocean temperature records, which makes it difficult to investigate the relationship (if any) between water temperature and Holocene grounding-line position. Ross Sea temperatures seem to have been warmer than present during the mid to late Holocene, based on radiocarbon dates of southern elephant seals (Hall et al., 2006) and on oxygen isotopes and Mg/Ca values of fossil shells (*Adamussium colbecki*; Braddock, 2014). Between ~8000-1000 yr BP, these seals, which require open water, had extensive rookeries along the western coast of the Ross Sea in an area now covered by perennial land-fast ice (Hall et al., 2006). At ~1000 yr BP, seal species changed dramatically, with southern elephant seals being replaced by other species (Weddell, crabeater), that require sea ice for their life histories (Bruyn et al., 2009). This significant change in sea ice over the past ~1000 years in the Ross Embayment may indicate that ocean temperatures decreased in the late Holocene, which may have helped to stabilize grounding-line retreat. δ18O and Mg/Ca measurements on fossil shells in the McMurdo Sound region exhibit the same pattern, with warmer than present temperatures since at least 6,500 yrs BP, and cooling by ~1,000 yrs BP (Braddock, 2014). This temperature decrease in the last millennium, however, appears to have occurred after the decrease in the rate of grounding-line retreat and thus cannot be implicated as a direct cause of slowed recession. In addition, it remains uncertain as to whether or not warm ocean water could infiltrate beneath the ice shelf as far as the southern Ross Embayment and affect melt rates at the grounding line.

Rising sea level is another potential mechanism for grounding-line retreat (Clark & Lingle, 1977). Eustatic sea-level rise occurred in response to global deglaciation, beginning gradually by ~26,000 yrs BP (Peltier & Fairbanks, 2006), with the highest rates of rise between ~16,000 - 9,000 yrs BP, punctuated by several rapid periods referred to as meltwater pulse events (Deschamps et al., 2012; Fairbanks, 1989; Lambeck et al., 2001). Ice thinning in the Ross Embayment at ~13,000 yrs BP may coincide with increasing eustatic sea level, but most of this sea-level rise occurred before any rapid recession in the Ross Embayment (Hall et al., 2015). Additionally, local sea level was falling in the southern Ross Sea by the time of grounding-line retreat due to isostatic uplift (Briggs et al., 2014; Ivins & James, 2005; Meur & Huybrechts, 1996; Whitehouse et al., 2012). Thus, local sea-level lowering may have offset the effect of eustatic sea-level rise and contributed to the stabilization of the ice sheet in the late Holocene.

Sediment wedges near the Siple Coast grounding line are also thought to provide stabilization against changes in sea level on the order of several meters (Alley et al., 2007). In addition, modeling based on surveys done on Whillans Ice Stream, just inland of the present grounding line, shows a region of till compression that also results in grounding-line stabilization (Christianson et al., 2013). However, these basal sediment conditions may not occur farther to the west along the TAM, and the lower basal melt rates in the southern Ross Embayment as opposed to the Siple Coast may result in fewer sediment wedges (Christianson et al., 2016).

Based on the potential mechanisms described above, a marine mechanism likely drove the deglaciation of the Ross Embayment, but exactly how that occurred is uncertain. Global deglaciation led to a higher and warmer ocean, which would have favored grounding-line retreat. Deepening of the sea floor inland of the continental shelf edge in the embayment may have further perpetuated retreat. However, isostatic rebound is thought to have led to local relative sea-level drop (Briggs et al., 2014; Ivins & James, 2005; Whitehouse et al., 2012), counteracting the effect of the rising global ocean. Moreover, a large portion of global sea-level rise was complete before Ross Sea deglaciation even began (Fairbanks, 1989), and very little eustatic change has occurred over the past several thousand years, the timeframe of my data. Thus, the exact relationship between grounding-line retreat and sea level remains complicated. One possibility, however, is that isostatic rebound may have allowed the grounding line to become more stable in the late Holocene as water shallowed. The increase in accumulation until ~2,000 yrs BP (Koutnik et al., 2016) probably aided in this stabilization, particularly if ocean temperatures were beginning to cool.

Table 4. Forcing Mechanism Comparison. Assessment of potential forcing mechanisms for retreat of ice in the Ross Embayment

Forcing Mechanism	Rapid Ice Recession 9,000-7,500 yrs BP	Slow recession ~4,500-3,000 yrs BP
Accumulation	• High accumulation in the Holocene may have delayed, but did not stop ice recession in the Ross Sea	• Maximum accumulation rate of the Holocene between ~4,000-2,000 yrs BP may have slowed recession
Ocean Temperature	• Warmer-than-present Ross Sea temperatures between ~8,000-1,000 yrs BP may have aided grounding-line retreat	• Colder Ross Sea temperatures by 1,000 yr BP than during the mid to late Holocene may have aided in grounding-line stabilization. • Slowly declining ocean temperatures throughout the Holocene may have slowed recession • The ocean temperature decrease appears to have occurred after the decrease in the rate of grounding-line retreat • Uncertainty as to whether temperature changes in the Ross Sea could affect the grounding line so far south and inland of the RIS
Sea-Level Rise	• Rising global sea levels may have aided ice recession • Most sea-level rise occurred before any rapid retreat response in the Ross Embayment • Local sea level was falling in the southern Ross Sea by the time of grounding-line retreat due to isostatic uplift	• Local sea-level lowering due to isostatic uplift during the Holocene, causing shallowing and potential grounding-line stabilization
Bathymetry	• Deepening of the sea floor inland of the continental shelf edge in the Ross Embayment could promote more rapid recession • Possible presence of sediment wedges near the grounding line could delay retreat	• Possibility of a sediment wedge causing local shallowing and grounding-line stabilization

4.3 Implications for Behavior of the AIS

The current increase in the speed of some ice streams (Conway et al., 2002) and loss of glacier and ice shelf volume in the Amundsen Sea sector and on the Antarctic Peninsula (De Angelis & Skvarca, 2003; Joughin et al., 2014a; Rignot et al., 2014; Scambos et al., 2004) are causing instability along the periphery of the AIS. If the processes causing ice-shelf breakup on the Antarctic Peninsula or the incursions of warm water to the grounding line in the Amundsen Sea were to extend farther south, they could result in the loss of the RIS, which would greatly affect the Siple Coast ice streams which drain that sector of the WAIS (Mercer, 1978). Given this possibility, as well as the fact that the grounding position of the WAIS is below sea level and that the bed becomes deeper inland, there is concern that the ice sheet could experience rapid retreat, perhaps parallel to that seen in the Ross Embayment during parts of the Holocene (Hughes, 1973). The data from this study indicate that the grounding line has likely remained just south of Scott Glacier for the last 3,000 years and may be stable at present. My data also show that some mechanism delayed retreat in the southern Ross Embayment relative to global deglaciation and caused slower retreat in the late Holocene than in the early Holocene. Identification of this mechanism is a priority, because if its effect should wane, ice recession may begin anew. It is also important to note that while my record suggests only gradual change in the late Holocene, the mid-Holocene was a period of instability and grounded ice reconfiguration in the Ross Embayment. Thus, the Ross Sea sector of the AIS is capable of big changes within short periods of time.

In the future, accumulation is likely to increase given warming in the Antarctic. However, it is uncertain whether this effect will cause ice-sheet growth or whether it may perpetuate ongoing peripheral loss if it results in a steepened profile causing a higher driving stress (Winkelmann et al., 2012). It is also unclear whether increasing ocean and atmospheric temperatures (Mercer, 1978; Russell et al., 2006; Schneider et al., 2006; Yin et al., 2011), as well as shifting of wind and ocean circulation patterns (Russell et al., 2006; Toggweiler & Russell, 2008), may cause greater instability than seen over the Holocene. As a result, while my data suggest stability in this sector of Ross Embayment over the last ~3,000 years, it's important to consider how forcing mechanisms influencing the ice sheet at present and in the future may differ in rate and/or magnitude from those which occurred at the end of the last ice age.

CHAPTER 5

CONCLUSIONS

5.1 Key Findings of this Thesis

- Glacial deposits on nunataks adjacent to the Ross Embayment allow reconstruction of former ice extent, elevation, and flow direction both during the LGM and during the deglaciation. These deposits provide context for the behavior of the AIS during these times.
- Radiocarbon dating of ancient algae deposited in former ice-dammed ponds allows me to investigate the timing and nature of ice recession at my field sites. My radiocarbon chronologies show little change in pond elevation over the past several thousand years, suggesting that ice had reached close to its present level and the Ross Sea grounding line had passed to the south of my sites. The oldest radiocarbon dates at Witalis Peak, Duncan Valley, and Mt. Mason represent minimum-limiting ages for the timing of grounding-line retreat past each respective site.
- Deglaciation in the southern Ross Embayment occurred between ~4200-2900 yrs BP. Specifically, the grounding line passed Duncan Mountains sometime shortly before ~4200 yr BP and Witalis Peak before ~2900 yr BP (but not earlier than ~3400 yr BP, a maximum limiting age on grounding-line recession at nearby Scott Glacier).
- Prior studies show that the deglaciation was marked by an initial period of rapid retreat, indicative of instability in this sector of the AIS. My data show that this was followed by a more gradual period of retreat in the late Holocene, with possible stabilization of the grounding line shortly after ~3000 yrs BP when it retreated to near its current position on the Siple Coast in the vicinity of Mercer Ice Stream.

- The timing of grounding-line retreat does not correspond closely with the largest post-LGM changes in global sea level or ocean temperature. The effects of increased accumulation, falling local sea level due to isostatic rebound, and potentially the slow response of an ice sheet of this magnitude, may have delayed any significant retreat until after 13,000 yr BP.
- The data from this study, as well as from Scott Glacier, indicate that the grounding line in the southern Ross Embayment reached close to its present position at ~3,000 yrs and probably has remained there ever since. Thus, the WAIS grounding line may be relatively stable in the Ross Sea sector at present.

BIBLIOGRAPHY

Ackert, R. (2008). Swinging gate or Saloon doors: Do we need a new model of Ross Sea deglaciation? In *Fifteenth West Antarctic Ice Sheet Meeting*. Sterling, Virginia.

Ackert, R. P., Barclay, D. J., Borns, H. W., Calkin, P. E., Kurz, M. D., Fastook, J. L., & Steig, E. J. (1999). Measurements of Past Ice Sheet Elevations in Interior West Antarctica. *Science*, *286*(5438), 276–280.

Allard, S., Hall, B. L., Denton, G. H., Bamber, J. L., Riva, R. E. M., Vermeersen, B. L. A., … Cold, U. S. A. (2013). Paleocean circulation during the lst deglaciation: A bipolar seasaw? *Quaternary Science Reviews*, *13*(1), 384–398. https://doi.org/10.1016/j.quascirev.2012.06.010

Alley, R. B., Anandakrishnan, S., Dupont, T. K., Parizek, B. R., Pollard, D., Alley, R. B., … Dupont, T. K. (2007). Effect of Sedimentation on Ice-Sheet Grounding-Line Stability, *315*(5820), 1838–1841.

Anderson, B. M., Hindmarsh, R. C. A., & Lawson, W. J. (2004). A modelling study of the response of Hatherton Glacier to Ross Ice Sheet grounding line retreat, *42*, 143–153. https://doi.org/10.1016/j.gloplacha.2003.11.006

Anderson, J. B., Conway, H., Bart, P. J., Witus, A. E., Greenwood, S. L., McKay, R. M., … Stone, J. O. (2014). Ross Sea paleo-ice sheet drainage and deglacial history during and since the LGM. *Quaternary Science Reviews*, *100*, 31–54. https://doi.org/10.1016/j.quascirev.2013.08.020

Anderson, R. F., Ali, S., Bradtmiller, L. I., Nielsen, S. H., Fleisher, M. Q., Anderson, B. E., & Burckle, L. H. (2009). Rise in Atmospheric CO 2. *Science*, *323*(March), 1443–1448.

Bamber, J. L., Riva, R. E. M., Vermeersen, B. L. A., & LeBrocq, A. M. (2009). Reassessment of the Potential Sea-Level Rise from a Collapse of the West Antarctic Ice Sheet. *Science*, *324*(5929), 901–903. https://doi.org/10.1126/science.1169335

Baroni, C., & Hall, B. L. (2004). A new Holocene relative sea-level curve for Terra Nova Bay , Victoria Land , Antarctica, *19*, 377–396. https://doi.org/10.1002/jqs.825

Bassett, S. E., Milne, G. A., Bentley, M. J., & Huybrechts, P. (2007). Modelling Antarctic sea-level data to explore the possibility of a dominant Antarctic contribution to meltwater pulse IA. *Quaternary Science Reviews*, *26*(17–18), 2113–2127. https://doi.org/10.1016/j.quascirev.2007.06.011

Bliss, A. K., Cuffey, K. M., & Kavanaugh, J. L. (2011). Sublimation and surface energy budget of Taylor Glacier , Antarctica, *57*(204), 684–696.

Bockheim, J. G., Wilson, S. C., Denton, G. H., Andersen, B. G., & Stuiver, M. (1989). Late Quaternary ice-surface fluctuations of Hatherton Glacier, Transantarctic Mountains. *Quaternary Research*, *31*(2), 229–254. https://doi.org/10.1016/0033-5894(89)90007-0

Braddock, S. (2014). *Holocene Sea-Surface Temperatures in the McMurdo Sound Region , Antarctica , Reconstructed from Isotope Records of Adamussium colbecki*.

Briggs, R. D., Pollard, D., & Tarasov, L. (2014). A data-constrained large ensemble analysis of Antarctic evolution since the Eemian. *Quaternary Science Reviews*, *103*, 91–115. https://doi.org/10.1016/j.quascirev.2014.09.003

Bromley, G. R. M., Hall, B. L., Stone, J. O., & Conway, H. (2012). Late Pleistocene evolution of Scott Glacier, southern Transantarctic Mountains: Implications for the Antarctic contribution to deglacial sea level. *Quaternary Science Reviews*, *50*, 1–13. https://doi.org/10.1016/j.quascirev.2012.06.010

Bromley, G. R. M., Hall, B. L., Stone, J. O., Conway, H., & Todd, C. E. (2010). Late Cenozoic deposits at Reedy Glacier, Transantarctic Mountains: implications for former thickness of the West Antarctic Ice Sheet. *Quaternary Science Reviews*, *29*(3–4), 384–398. https://doi.org/10.1016/j.quascirev.2009.07.001

Bruyn, M. De, Hall, B. L., Chauke, L. F., Baroni, C., Koch, P. L., & Hoelzel, A. R. (2009). Rapid Response of a Marine Mammal Species to Holocene Climate and Habitat Change, *5*(7). https://doi.org/10.1371/journal.pgen.1000554

Burgener, J. D. (1975). *Petrography of the Queen Maud Batholith, Central Transantarctic Mountains, Ross Dependency, Antarctica*.

Christianson, K., Jacobel, R. W., Horgan, H. J., Alley, R. B., Anandakrishnan, S., Holland, D. M., & Dallasanta, K. J. (2016). Basal conditions at the grounding zone of Whillans Ice Stream, from ice-penetrating radar. *Journal of Geophysical Research: Earth Surface*, *121*, 1954–1983. https://doi.org/10.1002/2015JF003806.Received

Christianson, K., Parizek, B. R., Alley, R. B., Horgan, H. J., Jacobel, R. W., Anandakrishnan, S., … Muto, A. (2013). Ice sheet grounding zone stabilization due to till compaction. *Geophysical Research Letters*, *40*(20), 5406–5411. https://doi.org/10.1002/2013GL057447

Clapperton, C. M., & Sugden, D. E. (1988). Holocene Glacier Fluctuation in South America and Antarctica. *Quaternary Science Reviews*, *7*(1987), 185–198.

Clark, J. A., & Lingle, C. S. (1977). Future sea-level changes due to West Antarctic ice sheet fluctuations. *Nature*, *269*(5625), 206–209. https://doi.org/10.1038/269206a0

Conway, H., Catania, G., Raymond, C. F., Gades, A. M., Scambos, T. A., & Engelhardt, H. (2002). Switch of flow direction in an Antarctic ice stream. *Nature*, *419*(465–467), 1192–1195.

Conway, H., Hall, B. L., Denton, G. H., Gades, A. M., & Waddington, E. D. (1999). Past and Future Grounding-Line Retreat of the West Antarctic Ice Sheet, *286*(5438), 280–283.

Cook, A. J., & Vaughan, D. G. (2010). Overview of areal changes of the ice shelves on the Antarctic Peninsula over the past 50 years. *The Cryosphere*, *4*, 77–98.

Cook, C. P., Flierdt, T. Van De, Williams, T., Hemming, S. R., Iwai, M., Kobayashi, M., … Galindo, A. L. (2013). Dynamic behaviour of the East Antarctic ice sheet during Pliocene warmth, *6*(September), 765–769. https://doi.org/10.1038/ngeo1889

Crosta, X., Sturm, A., Armand, L., & Pichon, J. J. (2004). Late Quaternary sea ice history in the Indian sector of the Southern Ocean as recorded by diatom assemblages. *Marine Micropaleontology*, *50*(3–4), 209–223. https://doi.org/10.1016/S0377-8398(03)00072-0

Cuffey, K. M., Clow, G. D., Steig, E. J., Buizert, C., Fudge, T. J., Koutnik, M., & Waddington, E. D. (2016). Deglacial temperature history of West Antarctica, *113*(50), 14249–14254. https://doi.org/10.1073/pnas.1609132113

De Angelis, H., & Skvarca, P. (2003). Glacier Surge after Ice Shelf Collapse. *Science*, *299*(5612), 1560–1562.

Denton, G. H., Anderson, R. F., Toggweiler, J. R., Edwards, R. L., Schaefer, J. M., & Putnam, A. E. (2010). The Last Glacial Termination. *Science*, *328*(June), 1652–1656. https://doi.org/10.1126/science.1184119

Denton, G. H., Bockheim, J. G., Wilson, S. C., & Stuiver, M. (1989). Late Wisconsin and Early Holocene Glacial History , Inner theories , particularly with respect to the relative timing of climate changes between polar hemispheres . To address these issues , we describe here late Quaternary paleoclimate , ice- volume chan. *Quaternary Research*, *31*, 151–182.

Denton, G. H., & Hughes, T. J. (2000). Reconstruction of the Ross Ice Drainage System, Antarctica, at the Last Glacial Maximum. *Geografiska Annaler. Series A, Physical Geography*, *82*, 143–166.

Denton, G. H., & Hughes, T. J. (2002). Reconstructing the Antarctic Ice Sheet at the Last Glacial Maximum, *21*, 193–202.

Denton, G. H., Sugden, D. E., Marchant, D. R., Hall, B. L., Wilch, T. I., Denton, G. H., … Wilch, T. I. (1993). East Antarctic Ice Sheet Sensitivity to Pliocene Climatic Change from a Dry Valleys Perspective. *Geografiska Annaler. Series A, Physical Geography*, *75*(4), 150–204.

Deschamps, P., Durand, N., Bard, E., Hamelin, B., Camoin, G., Thomas, A. L., … Yokoyama, Y. (2012). Ice-sheet collapse and sea-level rise at the Bølling warming 14,600 years ago. *Nature*, *483*(7391), 559–564. https://doi.org/10.1038/nature10902

Dutrieux, P., Rydt, J. De, Jenkins, A., Holland, P. R., Ha, H. K., Lee, S. H., … Schroder, M. (2014). Strong Sensitivity of Pine Island Ice-Shelf Melting to Climatic Variability. *Science*, *343*(January), 174–179.

Fahnestock, M. A., Scambos, T. A., Bindschadler, R., & Kvaran, G. (2000). A millennium of variable ice flow recorded by the Ross Ice Shelf, Antarctica. *Journal of Glaciology*, *46*, 652–664.

Fairbanks, R. G. (1989). A 17,000-year glacio-eustatic sea level record: influence of glacial melting rates on the Younger Dryas event and deep-ocean circulation. *Nature*, *342*, 637–642.

Fretwell, P., Pritchard, H. D., Vaughan, D. G., Bamber, J. L., Barrand, N. E., Bell, R., & Bianchi, C. (2013). The Cryosphere Bedmap2 : improved ice bed , surface and thickness datasets for Antarctica, 375–393. https://doi.org/10.5194/tc-7-375-2013

Gombiner, J., Stone, J. O. H., & Hall, B. L. (n.d.). Surface exposure age dating in the southern Transantarctic Mountains.

Hall, B. L., Baroni, C., & Denton, G. H. (2004). Holocene relative sea-level history of the Southern Victoria Land Coast, Antarctica. *Global and Planetary Change*, *42*(1–4), 241–263. https://doi.org/10.1016/j.gloplacha.2003.09.004

Hall, B. L., Bromley, G. R. M., Stone, J. O. H., & Conway, H. (2016). Holocene ice recession at Polygon Spur, Reedy Glacier, Antarctica. *The Holocene*, 1–8. https://doi.org/10.1177/0959683616652708

Hall, B. L., & Denton, G. H. (2000). Radiocarbon chronology of Ross Sea drift, eastern Taylor Valley, Antarctica; evidence for a grounded ice sheet in the Ross Sea at the last glacial maximum. *Geografiska Annaler. Series A: Physical Geography*, *82*(2–3), 305–336. https://doi.org/10.1111/j.0435-3676.2000.00127.x

Hall, B. L., Denton, G. H., Heath, S. L., Jackson, M. S., & Koffman, T. N. B. (2015). Accumulation and marine forcing of ice dynamics in the western Ross Sea during the last deglaciation. *Nature Geoscience*, *8*(8), 625–628. https://doi.org/10.1038/ngeo2478

Hall, B. L., Denton, G. H., Stone, J. O., & Conway, H. (2013). History of the grounded ice sheet in the Ross Sea sector of Antarctica during the Last Glacial Maximum and the last termination. *Geological Society, London, Special Publications*, *381*(1), 167–181. https://doi.org/10.1144/SP381.5

Hall, B. L., Hoelzel, A. R., Baroni, C., Denton, G. H., Boeuf, B. J. Le, Overturf, B., & To, A. L. (2006). Holocene elephant seal distribution implies warmer-than-present climate in the Ross Sea, *103*(27), 10213–10217.

Heirman, K., De Batist, M., Charlet, F., Moernaut, J., Chapron, E., Brümmer, R., … Urrutia, R. (2011). Detailed seismic stratigraphy of Lago Puyehue: Implications for the mode and timing of glacier retreat in the Chilean Lake District. *Journal of Quaternary Science*, *26*(7), 665–674. https://doi.org/10.1002/jqs.1491

Hendy, C. H., & Hall, B. L. (2006). The radiocarbon reservoir effect in proglacial lakes : Examples from Antarctica, *241*, 413–421. https://doi.org/10.1016/j.epsl.2005.11.045

Hughes, T. (2009). Modeling ice sheets from the bottom up. *Quaternary Science Reviews*, *28*(19–20), 1831–1849. https://doi.org/10.1016/j.quascirev.2009.06.004

Hughes, T. J. (1973). Is the West Antarctic Ice Sheet Disintegrating? *Journal of Geophysical Research*, *78*(33), 7884–7910. https://doi.org/10.1029/JC078i033p07884

Hulbe, C., & Fahnestock, M. (2007). Century-scale discharge stagnation and reactivation of the Ross ice streams , West Antarctica, *112*(January), 1–11. https://doi.org/10.1029/2006JF000603

Ivins, E. R., & James, T. S. (2005). Antarctic glacial isostatic adjustment : a new assessment, *17*(4), 541–553. https://doi.org/10.1017/S0954102005002968

Jackson, M. S. (2013). *Glacial history of Salmon Valley, Royal Society Range, Antarctica*.

Jackson, M. S., Hall, B. L., & Denton, G. H. (2017). Asynchronous behavior of the Antarctic Ice Sheet and local glaciers during and since Termination 1, Salmon Valley, Antarctica. *Earth and Planetary Science Letters*, *482*, 396–406. https://doi.org/10.1016/j.epsl.2017.11.038

Jones, R. S., Mackintosh, A. N., Norton, K. P., Golledge, N. R., Fogwill, C. J., Kubik, P. W., … Greenwood, S. L. (2015). Rapid Holocene thinning of an East Antarctic outlet glacier driven by marine ice sheet instability. *Nature Communications*, *6*. https://doi.org/10.1038/ncomms9910

Joughin, I., Smith, B. E., & Medley, B. (2014a). Marine Ice Sheet Collapse Potentially Under Way for the Thwaites Glacier Basin, West Antarctica. *Science*, *344*(6185). https://doi.org/10.1126/science.1249055

Joughin, I., Smith, B. E., & Medley, B. (2014b). Marine Ice Sheet Collapse Potentially Under Way for the Thwaites Glacier Basin, West Antarctica, (May), 735–739.

Kim, J. H., Crosta, X., Willmott, V., Renssen, H., Bonnin, J., Helmke, P., … Sinninghe Damsté, J. S. (2012). Holocene subsurface temperature variability in the eastern Antarctic continental margin. *Geophysical Research Letters*, *39*(6), 3–8. https://doi.org/10.1029/2012GL051157

Kimura, S., Jenkins, A., Dutrieux, P., Forryan, A., Naveira Garabato, A. C., & Firing, Y. (2016). Ocean mixing beneath Pine Island Glacier ice shelf, West Antarctica. *Journal of Geophysical Research: Oceans*, *121*(12), 8496–8510. https://doi.org/10.1002/2016JC012149

King, C. (2017). *Understanding Climate History and Ice Extent in the Mid- to High Latitudes of the Southern Hemisphere During the Last Glacial Maximum*.

Koutnik, M. R., Fudge, T. J., Conway, H., Waddington, E. D., Neumann, T. A., Cuffey, K. M., … Taylor, K. C. (2016). Holocene accumulation and ice flow near the West Antarctic Ice Sheet Divide ice core site. *Journal of Geophysical Research: Earth Surface*, *121*, 907–924.

Lambeck, K., Chappell, J., Lambeck, K., & Chappell, J. (2001). Sea Level Change through the Last Glacial Cycle Published by : American Association for the Advancement of Science Linked references are available on JSTOR for this article : Sea Level Change Through the Last Glacial Cycle, *292*(5517), 679–686.

Licht, K. J. (2004). The Ross Sea's contribution to eustatic sea level during meltwater pulse 1A. *Sedimentary Geology*, *165*(3–4), 343–353. https://doi.org/10.1016/j.sedgeo.2003.11.020

Masson, V., Vimeux, F., Jouzel, J., Morgan, V., Delmotte, M., Ciais, P., … Vaikmae, R. (2000). Holocene climate variability in Antartica based on 11 ice-core isotopic records. *Quaternary Research*, *54*(3), 348–358. https://doi.org/10.1006/qres.2000.2172

McGregor, V. R. (1965). Geology of the area between the Axel Heiberg and Shackleton Glaciers , Queen Maud Range , Antarctica. *New Zealand Journal of Geology and Geophysics*, *8*(2), 314–343. https://doi.org/10.1080/00288306.1965.10428114

McKay, R., Golledge, N. R., Maas, S., Naish, T., Levy, R., Dunbar, G., & Kuhn, G. (2016). Supplementary Methods; Antarctic marine ice-sheet retreat in the Ross Sea during the early Holocene. *Geology*. https://doi.org/10.1002/jqs.825.Cowan

Mckay, R. M., Dunbar, G. B., Naish, T. R., Barrett, P. J., Carter, L., & Harper, M. (2008). Retreat history of the Ross Ice Sheet (Shelf) since the Last Glacial Maximum from deep-basin sediment cores around Ross Island, *260*, 245–261. https://doi.org/10.1016/j.palaeo.2007.08.015

Members, W. D. P. (2013). Onset of deglacial warming in West Antarctica driven by local orbital forcing. *Nature*, *500*, 440. Retrieved from http://dx.doi.org/10.1038/nature12376

Mercer, J. H. (1978). West Antarctic Ice Sheet and CO2 Greenhouse Effect: a Threat of Disaster. *Nature*, *271*, 321–325.

Meur, E., & Huybrechts, P. (1996). A comparison of different ways of dealing with isostasy : examples from modelling the Antarctic ice sheet during the last glacial cycle.

Miller, K. G., Wright, J. D., Browning, J. V., Kulpecz, A., Kominz, M., Naish, T. R., … Sosdian, S. (2012). High tide of the warm pliocene: Implications of global sea level for Antarctic deglaciation. *Geology*, *40*(5), 407–410. https://doi.org/10.1130/G32869.1

Parish, T. R., & Bromwich, D. H. (1998). A Case Study of Antarctic Katabatic Wind Interaction with Large-Scale Forcing *. *American Meteorological Society*, *126*, 199–209.

Parizek, R., Alley, B., & Hulbe, L. (2003). Subglacial thermal balance permits ongoing grounding-line retreat along the Siple Coast of West Antarctica, (2001), 251–256.

Passchier, S. (2001). Provenance of the Sirius Group and related Upper Cenozoic glacial deposits from the Transantarctic Mountains , Antarctica : relation to landscape evolution and ice-sheet drainage, *144*.

Peltier, W. R., & Fairbanks, R. G. (2006). Global glacial ice volume and Last Glacial Maximum duration from an extended Barbados sea level record, *25*, 3322–3337. https://doi.org/10.1016/j.quascirev.2006.04.010

Pollard, D., Deconto, R. M., & Alley, R. B. (2015). Potential Antarctic Ice Sheet retreat driven by hydrofracturing and ice cliff failure. *Earth and Planetary Science Letters*, *412*, 112–121. https://doi.org/10.1016/j.epsl.2014.12.035

Price, S. F., Conway, H., & Waddington, E. D. (2007). Evidence for late Pleistocene thinning of Siple Dome , West Antarctica, *112*(February), 1–13. https://doi.org/10.1029/2006JF000725

Putnam, a. E., & Schaefer, J. M. (2013). The Last Glacial Maximum at 44° S documented by a 10 Be moraine chronology at Lake Ohau, Southern Alps of New Zealand. *Quaternary Science …*, *62*, 114–141. Retrieved from http://www.sciencedirect.com/science/article/pii/S0277379112004386

Putnam, A. E., Schaefer, J. M., Denton, G. H., Barrell, D. J. A., Andersen, B. G., Koffman, T. N. B., … Ladig, K. L. (2013). Warming and glacier recession in the Rakaia valley, Southern Alps of New Zealand, during Heinrich Stadial 1. *Earth and Planetary Science Letters*, *382*, 98–110. https://doi.org/10.1016/j.epsl.2013.09.005

Reimer, P. J., Bard, E., Bayliss, A., Beck, J. W., Blackwell, P. G., Bronk, C., … Edwards, R. L. (2013). Intcal13 and marine13 radiocarbon age calibration curves 0 – 50,000 years cal bp, *55*(4).

Rignot, E., Mouginot, J., Morlighem, M., Seroussi, H., & Scheuchl, B. (2014). Widespread , rapid grounding line retreat of Pine Island , Thwaites , Smith , and Kohler glaciers , West Antarctica , 3502–3509. https://doi.org/10.1002/2014GL060140.Received

Russell, J. L., Dixon, K. W., Gnanadesikan, A., Stouffer, R. J., & Toggweiler, J. R. (2006). The Southern Hemisphere Westerlies in a Warming World : Propping Open the Door to the Deep Ocean. *Journal of Climate*, *19*, 6382–6390.

Scambos, T. A., Bohlander, J. A., Shuman, C. A., & Skvarca, P. (2004). Glacier acceleration and thinning after ice shelf collapse in the Larsen B embayment, Antarctica. *Geophysical Research Letters*, *31*(18), 2001–2004. https://doi.org/10.1029/2004GL020670

Scherer, R. P., Deconto, R. M., Pollard, D., & Alley, R. B. (2016). Windblown Pliocene diatoms and East Antarctic Ice Sheet retreat, 1–9. https://doi.org/10.1038/ncomms12957

Schneider, D. P., Steig, E. J., Ommen, T. D. Van, Dixon, D. A., Mayewski, P. A., Jones, J. M., & Bitz, C. M. (2006). Antarctic temperatures over the past two centuries from ice cores, *33*(August), 1–5. https://doi.org/10.1029/2006GL027057

Shepherd, A., Wingham, D., & Rignot, E. (2004). Warm ocean is eroding West Antarctic Ice Sheet. *Geophysical Research Letters*, *31*(23), 1–4. https://doi.org/10.1029/2004GL021106

Simpson, G. C. (1934). World climate during the Quaternary period. *Quaternary Journal of the Royal Meteorological Society*, *60*, 425–475.

Skvarca, P., De Angelis, H., & Zakrajsek, A. F. (2004). Climatic conditions , mass balance and dynamics of Larsen B ice shelf , Antarctic Peninsula , prior to collapse. *Annals of Glaciology*, *39*(1), 557–562.

Spector, P., Stone, J., Cowdery, S., Hall, B., Conway, H., & Bromley, G. (2017). Rapid early-Holocene deglaciation in the Ross Sea , Antarctica. https://doi.org/10.1002/2017GL074216

Stearns, L. A. (2011). Dynamics and mass balance of four large East Antarctic outlet glaciers, *52*(59), 116–126.

Stearns, L., & Hamilton, G. (2005). A new velocity map for Byrd Glacier , East Antarctica , from sequential ASTER satellite imagery, *1*(2002), 71–76.

Steig, E. J., Ding, Q., Battisti, D. S., & Jenkins, A. (2012). Tropical forcing of Circumpolar Deep Water Inflow and outlet glacier thinning in the Amundsen Sea Embayment , West Antarctica, (53), 19–28. https://doi.org/10.3189/2012AoG60A110

Stuiver, M., Denton, G. H., & Hughes, T. J. (1981). History of the marine ice sheet in West Antarctica during the last glaciation: A working hypothesis. In *The Last Great Ice Sheets* (pp. 319–436). New York: Wiley-Interscience.

Todd, C., Stone, J., Conway, H., Hall, B., & Bromley, G. (2010). Late Quaternary evolution of Reedy Glacier, Antarctica. *Quaternary Science Reviews*, *29*(11–12), 1328–1341. https://doi.org/10.1016/j.quascirev.2010.02.001

Toggweiler, J. R., & Russell, J. L. (2008). Ocean Circulation in a warming climate. *Nature*, *451*(January), 286–288. https://doi.org/10.1002/2015JF003668.Received

Vihma, T., Tuovinen, E., & Savijärvi, H. (2011). Interaction of katabatic winds and near - surface temperatures in the Antarctic, *116*(August), 1–14. https://doi.org/10.1029/2010JD014917

Weber, M. E., Clark, P. U., Kuhn, G., Timmermann, A., Sprenk, D., Gladstone, R., … Ohlwein, C. (2014). Millennial-scale variability in Antarctic ice-sheet discharge during the last deglaciation. *Nature*, *510*(7503), 134–138. https://doi.org/10.1038/nature13397

Weertman, J. (1974). Stability of the junction of an ice sheet and an ice shelf. *Journal of Glaciology*, *13*(67), 3–11. https://doi.org/10.3198/1974JoG13-67-3-11

Weertman, J. (1976). Glaciology's grand unsolved problem. *Nature*, *260*(March 25), 284–286. https://doi.org/10.1038/261403a0

Whitehouse, P. L., Bentley, M. J., & Le, A. M. (2012). A deglacial model for Antarctica : geological constraints and glaciological modelling as a basis for a new model of Antarctic glacial isostatic adjustment. *Quaternary Science Reviews*, *32*, 1–24. https://doi.org/10.1016/j.quascirev.2011.11.016

Winkelmann, R., Levermann, A., Martin, M. A., & Frieler, K. (2012). Increased future ice discharge from Antarctica owing to higher snowfall. *Nature*, *492*(7428), 239–242. https://doi.org/10.1038/nature11616

Winnick, M. J., & Caves, J. K. (2015). Oxygen isotope mass-balance constraints on Pliocene sea level and East Antarctic Ice Sheet stability, *43*(10), 879–882. https://doi.org/10.1130/G36999.1

Yin, J., Overpeck, J. T., Griffies, S. M., Hu, A., Russell, J. L., & Stouffer, R. J. (2011). Different magnitudes of projected subsurface ocean warming around Greenland and Antarctica. *Nature Geoscience*, *4*(8), 524–528. https://doi.org/10.1038/nphys1189

Zwinger, T., Malm, T., Schafer, M., Stenberg, R., & Moore, J. C. (2015). Numerical simulations and observations of the role of katabatic winds in the creation and maintenance of Scharffenbergbotnen blue ice area , Antarctica. *The Cryosphere*, *9*, 1415–1426. https://doi.org/10.5194/tc-9-1415-2015

BIOGRAPHY OF THE AUTHOR

Jill Pelto was born in Worcester, MA, on April 2, 1993. She graduated from West Boylston High School in 2011. From 2009 to the present she has worked every August with her father, Dr. Mauri Pelto, on his North Cascade Glacier Climate Project. In December of 2015, Jill received a Bachelor of Arts in Earth and Climate Sciences, and a Bachelor of Arts in Studio Art, at the University of Maine at Orono. She graduated with High Honors in the Honors College, after completion of an undergraduate Thesis on the communication of science through art. During her undergraduate studies, she worked with Dr. Brenda Hall in the Dry Valleys and Royal Society Range in Antarctica, and in the Falkland Islands. Following graduation, Jill continued to pursue scientific art, and worked with her brother, PhD candidate Ben Pelto, on his research with the University of Northern British Columbia on glaciers in the province. She began her graduate studies at the University of Maine at Orono in the Fall of 2016, concentrating in glacial geomorphology. Jill is a candidate for the Master of Science degree in Earth and Climate Science from the University of Maine in August 2018.